

Research Paper

Optimizing energy supply superstructure for plastic waste gasification systems: minimizing life cycle environmental impacts with AI models

Qiming Qian^a, Yusha Hu^a, Jingzheng Ren^{a,*}, Chang He^b^a Research Institute for Advanced Manufacturing, Department of Industrial and Systems Engineering, The Hong Kong Polytechnic University, Hong Kong SAR, China^b School of Materials Science and Engineering, Guangdong Engineering Centre for Petrochemical Energy Conservation, Sun Yat-sen University, Guangzhou 510275, China

ARTICLE INFO

Keywords:

Plastic waste
Green process synthesis
Life cycle assessment
Network model
Machine learning
Surrogate-based optimization

ABSTRACT

This study optimizes the energy supply superstructure for plastic waste-to-energy system through path programming using machine learning models. Multiple fuel alternatives, carbon capture technologies, renewable energy driven water electrolysis techniques are incorporated into a mixed-integer nonlinear programming model. Surrogate model-based optimization strategy, which utilizes a machine learning model for regression, was applied to solve the path programming problem. The objective is to minimize the life cycle environmental impacts, with concurrent optimization of the surrogate model's hyperparameters. Feature importance analysis identifies the selection of carbon dioxide usage pathways as the most significant feature in determining the environmental impacts. 93.39 % of the CO₂ is favorable for compression for storage, while only 6.61 % is utilized for methanol synthesis. Negative global warming potential value is obtained for the optimal energy supply superstructure. Additionally, the study explores the interconnections between different midpoint environmental categories. Minimizing global warming potential and fossil resource scarcity impacts synergistically leads to significant increases in other environmental indicators. Conversely, minimizing human carcinogenic toxicity results in trade-offs with global warming potential. This research provides valuable insights into the environmental optimization of plastic waste valorization processes, highlighting the intricate balance required between different environmental objectives.

1. Introduction

Plastic waste pollution has emerged as a global environmental challenge. Each year, hundreds of millions of tons of plastic products are produced worldwide, with a substantial proportion ending up in mismanagement such as not recycled, incinerated, or landfills [1]. The accumulation of mismanaged plastic waste poses severe threats to marine ecosystems, wildlife, and human health.

In response to these challenges, plastic waste-to-energy technologies have gained increasing attentions as a promising strategy to mitigate the environmental impacts of plastic pollution. These technologies convert plastic waste into usable energy forms through processes such as pyrolysis, gasification, and incineration [2]. Among these, gasification is particularly noteworthy due to its ability to generate versatile and valuable syngas [3,4]. The composition and yield of syngas are influenced by various operational parameters, including the choice of gasifying agents [5], equivalence ratio [6], steam-to-oxygen ratio, and temperature. Previous studies have demonstrated that higher

temperature generally increase the yield of CO and H₂, while higher air-to-fuel equivalence ratios tend to decrease their concentrations [7]. Although the influence of gasification conditions on the syngas composition has been extensively investigated [8,9], there remains a need to validate these findings in larger, more integrated systems and to optimize the process for practical application.

Process synthesis, which involves the systematic design and optimization of chemical processes, plays a crucial role in developing efficient and sustainable plastic waste valorization systems. This approach encompasses the selection and arrangement of unit operations, reaction pathways, and separation processes to achieve optimal process flows. Techno-economic [10,11] and life cycle environmental impacts [12,13] are commonly used as key optimization objectives. Process synthesis can be categorized into deterministic approaches, where system units and their connections are predefined and operational conditions are optimized for energy, economic, and environmental performance [14–16], and uncertain process synthesis, which systematically evaluates a broad space of structural alternatives [17,18]. While deterministic approaches

* Corresponding author.

E-mail address: jzhren@polyu.edu.hk (J. Ren).

have been applied to both single-product and multi-generation systems [19,20], they often lack flexibility in adapting to changing optimization objectives. In contrast, superstructure optimization enables the exploration of alternative process configurations, but its application to plastic waste management remains underexplored.

Traditional approaches to modeling and solving network optimization problems in process systems engineering typically involve formulation of large-scale mixed-integer nonlinear programming models, which are then solved using numerical optimization algorithms and commercial solvers to determine the optimal values of decision variables [21]. To address the inherent computational complexity of these models, researchers often introduce simplifying assumptions—most notably, linear approximations of process units and relationships [17,22,23]. While such linearization facilitates tractable solutions, it can compromise the accuracy and fidelity of the resulting process designs. Consequently, many existing studies rely on linear models for operating units and depend heavily on commercial solvers, which may limit the exploration of more complex or realistic process behaviors [24,25]. To overcome these limitations, advanced strategies have been developed, including the use of surrogate models. Surrogate models serve as computational efficient approximations of expensive first-principle models that transport phenomena, thermodynamics, and reaction kinetics in alternative process units [26,27]. These studies typically concentrate on constructing surrogate models to approximate the performance of individual process unit or pathways, and optimization is performed to identify the most efficient process path. Such approaches have been demonstrated the potential of surrogate modeling to reduce computational burden. Despite these advances, most existing research still relies on linear assumptions and stepwise optimization using commercial solvers. Importantly, there remains a notable research gap in tackling the simultaneous optimization of both network structure (integer variables) and operating conditions (continuous variables) for entire process networks using surrogate-based, derivative-free optimization methods. This gap is particularly evident in the context of plastic waste treatment, where integrated and flexible optimization frameworks are needed to address system complexity and nonlinearity.

The primary goal of this study is to develop and demonstrate an advanced optimization framework for the design and operation of gasification-based plastic waste-to-energy networks. Specially, this study aims to simultaneously optimizes the core operating variables of the gasification process and the binary variables that define the optimal structure of the downstream utility supply chain. Furthermore, addressing the limitations of conventional mathematical programming approaches, which often rely on linear assumptions and commercial solvers, this study employs a surrogate-based, derivative-free optimization strategy. Finally, through the integration of life cycle assessment and machine learning technique, this research aims to provide a comprehensive assessment of the environmental performance of the optimized network, with a particular focus on minimizing multiple midpoint environmental indicators. This study makes several key contributions to the field of plastic waste valorization and process systems engineering:

1. An integrated superstructure model for energy supply network of plastic waste valorization is established, capturing the complexity and flexibility of potential process configurations.
2. A novel machine learning approach, utilizing decision tree models, is employed to approximate the mixed-integer nonlinear mathematical model of the network, effectively handling both continuous and discrete variables.
3. The interactions and trade-offs between different midpoint environmental indicators are systematically investigated, providing valuable insights for sustainable process design.

The remainder of this paper is organized as follows: Section 2.1 illustrates the energy supply superstructures for the plastic waste

gasification process. Section 2.2 presents the mathematical programming model of the energy supply superstructure. Section 2.3 describes the integrated optimization framework, including the formulation of the optimization problem and the implementation of derivative-free algorithms. Section 2.4 provides case studies demonstrating the application of the proposed methodology. Section 3 discusses the results of the case studies; Section 4 concludes the study by summarizing the main findings and limitations of this study.

2. Methods

2.1. Energy supply superstructure

A gasification-based network has been meticulously designed for the valorization of mixed plastic waste, as illustrated in Fig. 1. This network is bifurcated into two primary components: the upstream core gasification process and the downstream auxiliary systems. The core process, which involves the gasification of plastic waste to produce blue hydrogen, has been extensively explored in our previous research, as detailed in the reference [28]. The specific operating parameters for this process are enumerated in Section S1 of the Supplementary Material. The gasification employs steam and air techniques to generate a syngas stream (SYNG1) predominantly composed of carbon monoxide (CO), hydrogen (H₂), and carbon dioxide (CO₂). This syngas is subsequently cooled (SYNG2) and introduced into a water–gas shift reactor (R-WGS) to enhance hydrogen production. Building on our prior work, this process is now applied to a novel mixed plastic waste feedstock comprising 20 wt% of high-density polyethylene (HDPE), low-density polyethylene (LDPE), polypropylene (PP), polystyrene (PS), and polyethylene terephthalate (PET). The validation of the gasification process is documented in Section S1 of the Supplementary Material. Furthermore, the heat exchanger network has been optimized using the Aspen Energy Analyzer to minimize total costs before proceeding with the optimization of the entire network. The results are presented in Section S2 of the Supplementary Material. Following the optimization of the heat exchanger network, the outlet stream from the R-WGS (SYNG3) is utilized to recover heat for preheating steam streams (WATER1 & WATER2) prior to their entry into the gasifier and R-WGS, resulting in a 46.23 % reduction in heating demand. The raw syngas (SYNG4) undergoes further treatment within the downstream network systems. Various carbon capture techniques are considered for the pre-combustion carbon capture of SYNG4. It is assumed that the blue hydrogen derived from the purified gas can be employed in a gas turbine combined cycle system (GTCC), methanol synthesis, and as a final product. The captured CO₂ is intended for use in methanol synthesis, with the green hydrogen reactant sourced from different water electrolysis units. The life cycle impact is utilized as an objective to determine the optimal configuration of the network. Consequently, diverse renewable electricity and fuel alternatives are integrated into the network to assess environmental performance. Our aim is to ascertain the operating variables of the core gasification system while considering the structure of the downstream supply chain. This study investigates the influence of the downstream supply chain on the operating conditions of the upstream process. The core gasification process is rigorously modeled in Aspen Plus to capture the effects of decision variables. However, the consumption of utilities and raw materials, as well as the direct emissions from the downstream units, are linearly correlated with their functional units, as concluded from other studies [29–32] and detailed in Section S3 of the Supplementary Material.

2.2. Life cycle impact assessment model

The life cycle assessment (LCA) for the process network model is conducted in accordance with the ISO 14040 [33] and 14044 [34] standards. To evaluate the environmental objectives of the network model, the ReCiPe 2016 Midpoint (H) [35] life cycle impact assessment

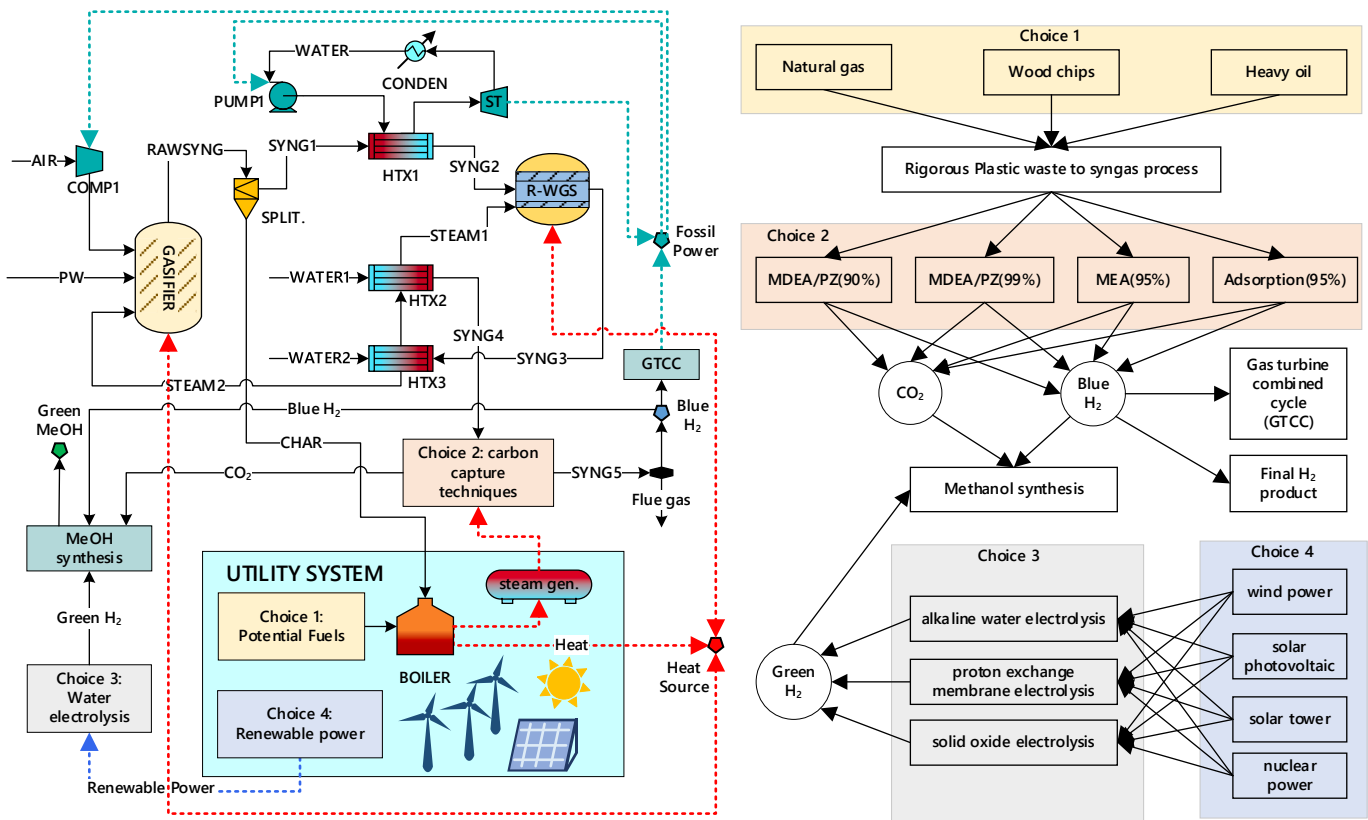


Fig. 1. Energy supply superstructure of the plastic waste valorization process.

model is employed. The functional unit for this assessment is defined as treatment of 1 kg mixed plastic waste. The system boundaries, illustrated in Fig. 2, delineate the life cycle inventory (LCI) into two distinct categories: foreground inventory and background inventory. Foreground inventories encompass direct emissions—gaseous, liquid, and solid—released into the air, water, and soil from all potential units within the system. It is assumed that flue gas undergoes combustion prior to atmospheric release, resulting in the formation of NO₂, SO₂, and CO₂ from nitrogen, sulfur, and carbon elements, respectively. Conversely, background inventory accounts for utility consumption and the avoidance of burdens associated with the final products. This study primarily considers utility streams such as cooling water, electricity, steam, and fuels. The potential final products of this plastic waste treatment network include blue hydrogen, methanol, and electricity. The Ecoinvent [36] database is utilized to provide background inventory.

2.2.1. Foreground inventory

In this analysis, it is assumed that combustible gas is released only after undergoing complete combustion. Consequently, the final form of carbon elements in the gaseous waste stream is carbon dioxide. There are four potential sources of direct CO₂ emissions $Emtg_{CO2}$: the combustion of biochar, which is the solid residue from the gasifier; the combustion of exhaust gas $Emtg_{CO2,gr}$; uncaptured gas from the carbon capture unit $Emtg_{CO2,cap}$; and emissions from the methanol synthesis unit $Emtg_{CO2,me}$, as delineated in Equation (1). Biochar, primarily composed of carbon, contributes to CO₂ emissions through its complete combustion. The CO₂ emissions resulting from this process are calculated based on the quantity of biochar Mas_{char} , considering the molar masses of CO₂ and biochar, which are 44 kg/mol and 12 kg/mol, respectively. This calculation provides a comprehensive understanding of the carbon footprint associated with the gasification process and highlights the significance of managing emissions from various sources within the

system.

$$Emtg_{CO2} = \frac{44}{12}Mas_{char} + Emtg_{CO2,gr} + Emtg_{CO2,cap} + Emtg_{CO2,me} \quad (1)$$

Balance of the CO₂ emissions from different carbon capture units is expressed in Eqs. (2) and (3).

$$Emtg_{CO2,cap} = \sum_{i=1}^C Emtg_{CO2,i} \times Syn_{CO2} \times Itcon_i \quad (2)$$

$$\sum_{i=1}^C Itcon_i = 1, 0 \leq Itcon_i \leq 1 \quad (3)$$

where $Emtg_{CO2,i}$ is the quantity of carbon dioxide emissions of carbon capture unit $i = \{cap1, cap2, cap3, cap4\}$ ($i \in C \subseteq D$), Syn_{CO2} is the number of carbon dioxide in the produced syngas from gasification of plastic waste, and $Itcon_i$ is the mass ratio of carbon dioxide input to the carbon capture technique i . D is the set of all potential equipment devices, and C is the subset of D . C includes the elements of all the potential carbon capture technologies.

In this process, nitrogen elements are derived from the gasification of plastic waste. The proximate and ultimate analyses of various types of plastic waste, sourced from different origins [37], provide insights into their composition. Within the gasifier, nitrogen elements are present in the form of NO and NO₂. During the combustion of flue gas, nitric oxide is converted into nitrogen dioxide. The quantity of direct nitrogen dioxide emissions $Emtg_{NO2}$ is initially determined from the process simulation results, as indicated in Eq. (4).

$$Emtg_{NO2} = Emtg_{NO2,gr} \quad (4)$$

Sulfur element in the process is from the gasification of plastic waste, where sulfur element exists in the form of hydrogen sulfide. The hydrogen sulfide is then converted into sulfur dioxide after the

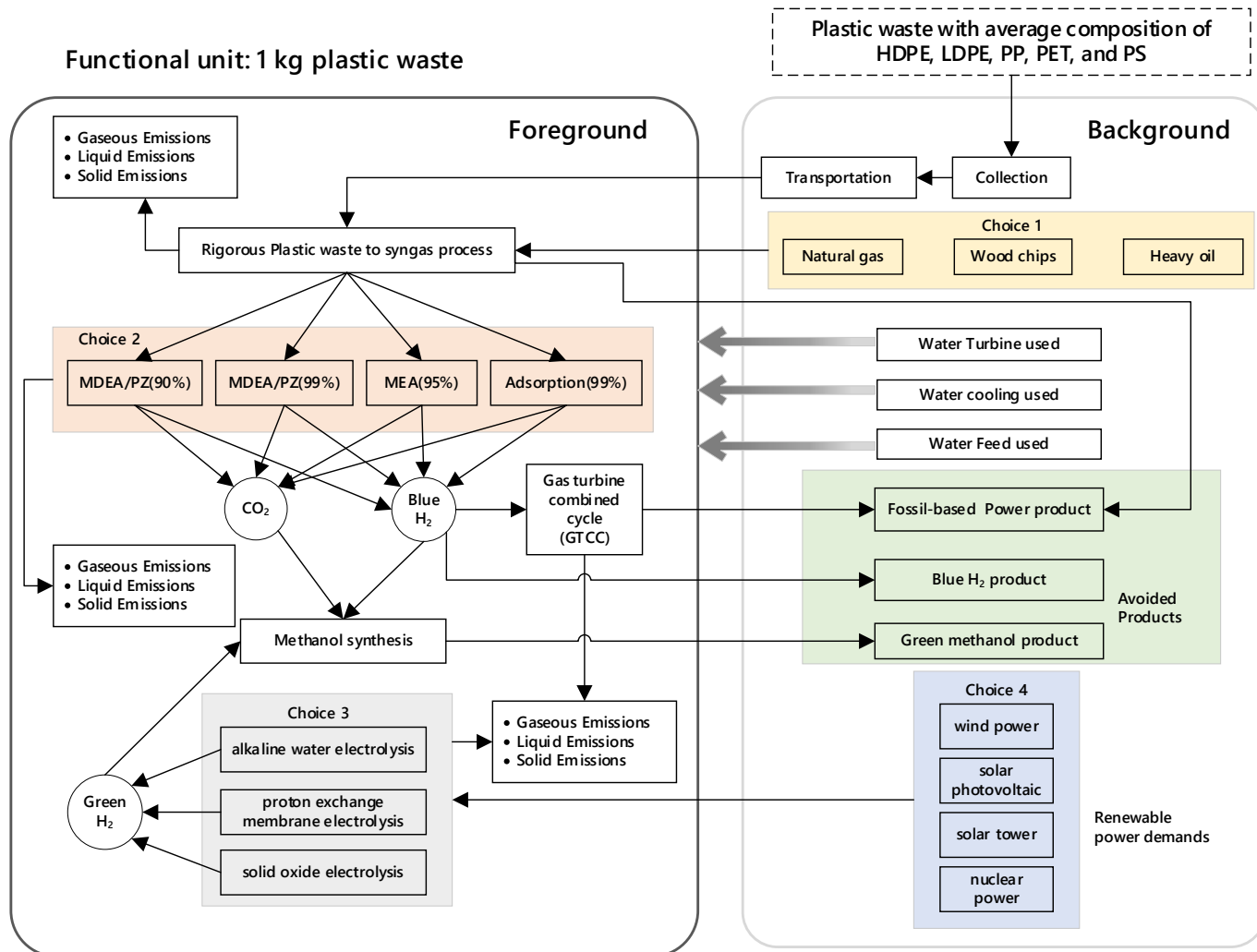


Fig. 2. System boundaries and functional unit for the plastic waste treatment network.

combustion of flue gas. The quantity of direct sulfur dioxide emissions $Emtg_{SO2}$ is initially obtained from the gasification of plastic waste, displayed in Eq. (5).

$$Emtg_{SO2} = Emtg_{SO2, gf} \quad (5)$$

Process of methanol synthesis from carbon dioxide and hydrogen is rigorously simulated in our previous work [32], where the number of utilities used and direct emissions per kg of CO_2 are extracted. The mass fraction of purified methanol products is over 99.5 %. Combustible gaseous exhausts, including hydrogen, methanol, and carbon monoxide, are assumed to undergo complete combustion prior to atmospheric release. As a result, the final emitted gases are expected to consist primarily of carbon dioxide and water. Despite this, there remains a release of methanol into the water within this unit, as represented in Eq. (6).

$$Emtl_{meoh} = Emtl_{meoh, me} \quad (6)$$

where $Emtl_{meoh}$ is the liquid methanol emission of the whole system, $Emtl_{meoh, me}$ is the liquid methanol released by the methanol synthesis and purification process.

Water consumption within the process can be categorized into three distinct types: water utilized by turbines Mtr_{twt} , water employed as cooling water Ut_{clw} , and water used as feed material Mtr_{wtr} . The water used as feed material has two primary sources: one originating from the gasification process and the other from the gas turbine combined cycle, as illustrated in Eq. (7).

$$Mtr_{twt} = Mtr_{twt, gt} + Mtr_{twt, gf} \quad (7)$$

Water is only used as feed material in the gasifier and water-gas-shift reactor of the gasification process, as shown in Eq. (8).

$$Mtr_{wtr} = Mtr_{wtr, gf} \quad (8)$$

The total consumption of cooling water in the process is comprised of four key components: the amount used in the gasification of plastics process $Ut_{clw, gf}$, the carbon capture process $Ut_{clw, cap}$, gas turbine combined cycle process $Ut_{clw, gt}$, and methanol synthesis and purification process $Ut_{clw, me}$, as detailed in Eq. (9).

$$Ut_{clw} = Ut_{clw, gf} + Ut_{clw, cap} + Ut_{clw, gt} + Ut_{clw, me} \quad (9)$$

Since the carbon capture unit has several alternative choices, the finalized cooling water consumption by this unit is calculated in Eq. (10).

$$Ut_{clw, cap} = \sum_{i=1}^c Ut_{clw, i} \times Itcon_i, i = \{cap1, cap2, cap3, cap4\} \in C \subseteq D \quad (10)$$

where $Ut_{clw, i}$ is the amount of cooling water consumption for carbon capture unit i .

2.2.2. Background inventory

Blue hydrogen generated by the gasification core process is allocated

in Eqs. (11) and (12).

$$Syn_{H2} = \sum_{h=1}^H Syn_{H2} \times fh_h \quad (11)$$

$$\sum_{h=1}^H fh_h = 1, 0 \leq fh_h \leq 1 \quad (12)$$

where Syn_{H2} is the amount of hydrogen in the syngas, and fh_h is the mass ratio of hydrogen input to the unit $h = \{me, gt, prd\}$ ($h \in H \subseteq D$).

Mass balance of the blue hydrogen is displayed in Eq. (13) to Eq. (15).

$$Mtr_{h2,me} = Prd_{gh2} + Syn_{H2} \times fh_{me} \quad (13)$$

$$Mtr_{h2,gt} = Syn_{H2} \times fh_{gt} \quad (14)$$

$$Prd_{h2} = Syn_{H2} \times fh_{prd} \quad (15)$$

where $Mtr_{h2,me}$ is the total amount of hydrogen consumed by the methanol synthesis process, Prd_{gh2} is the amount of green hydrogen produced by the water electrolysis technique, $Mtr_{h2,gt}$ is the amount of hydrogen consumed by the gas turbine, and Prd_{h2} is the amount of hydrogen delivered as final product, which will result in avoided environmental burdens.

Green hydrogen is produced by the water electrolysis and only used for green methanol synthesis in the network model. The mass balance of green hydrogen production is shown in Eqs. (16) and (17).

$$Prd_{gh2} = \sum_{w=1}^W Prd_{gh2,w} \times Itcon_w \quad (16)$$

$$\sum_{w=1}^W Itcon_w = 1, 0 \leq Itcon_w \leq 1 \quad (17)$$

where $Prd_{gh2,w}$ is the amount of green hydrogen produced by the water electrolysis techniques $w = \{ew1, ew2, ew3\}$ ($w \in W \subseteq D$), and $Itcon_w$ is the mass ratio of green hydrogen produced by the water electrolysis technique w . $ew1$ indicates the alkaline water electrolysis (AWE), $ew2$ refers to proton exchange membrane electrolysis (PEME), and $ew3$ is the solid oxide electrolysis with electric heaters (SOEC).

Except for the fuel supplied from the outer resources, the biochar produced by the system itself is assumed to be used as fuel supply preferentially. The amount of heat generated by biochar $Ut_{fuel,char}$ is calculated from the higher heating value hhv_{char} , which is 32.8 MJ/kg [38] for carbon, as shown in Eq. (18).

$$Ut_{fuel,char} = \frac{1000}{3600} Mas_{char} hhv_{char} \quad (18)$$

Biochar produced is first considered to combusted as fuel supply for the gasifier. The net heat consumption of gasifier Ut_{fuel,gsf_net} is calculated in Eq. (19).

$$Ut_{fuel,gsf_net} = Ut_{fuel,gsf} - Ut_{fuel,char} \quad (19)$$

where $Ut_{fuel,gsf}$ is the number of heat consumption of the gasifier, which is calculated by the balance of heat of reaction and generated by simulation software. If $Ut_{fuel,gsf}$ is positive, it means that the gasifier needs heat supply. Nevertheless, there is extra heat output of the gasifier, which is assumed to be fully converted into steams. Product steams will bring positive environmental effects. For the heat balance of the water-gas-shift reactor $Ut_{fuel,wgs}$, similar logical calculation is applied, as shown in Eqs. (20) and (21).

$$Ut_{fuel} = \begin{cases} Ut_{fuel,gsf_net} + Ut_{fuel,wgs} & \text{when } Ut_{fuel,gsf_net} \geq 0 \text{ and } Ut_{fuel,wgs} \geq 0 \\ 0 & \text{when } Ut_{fuel,gsf_net} < 0 \text{ and } Ut_{fuel,wgs} < 0 \end{cases} \quad (20)$$

$$Prd_{stm} = \begin{cases} -Ut_{fuel,gsf_net} - Ut_{fuel,wgs} & \text{when } Ut_{fuel,gsf_net} < 0 \text{ and } Ut_{fuel,wgs} < 0 \\ 0 & \text{when } Ut_{fuel,gsf_net} \geq 0 \text{ and } Ut_{fuel,wgs} \geq 0 \end{cases} \quad (21)$$

where Ut_{fuel} is the net fuel consumption of the whole system, in the form of heat. Prd_{stm} is the amount of heat generated by the gasifier and the water-gas-shift reactor.

Potential final products of the system include blue hydrogen Prd_{h2} , extra steam Prd_{stm} , green methanol Prd_{meth} , and fossil-based electricity Prd_{elec} . The green methanol is solely produced by the methanol synthesis and purification unit $Prd_{meth,me}$, while the electricity product is sourced from the gas turbine combined cycle unit $Prd_{elec,gt}$ and the gasification core process $Prd_{elec,gf}$, as depicted in Eq. (22) and Eq. (23).

$$Prd_{meth} = Prd_{meth,me} \quad (22)$$

$$Prd_{elec} = Prd_{elec,gt} + Prd_{elec,gf} \quad (23)$$

There are various potential fuel choices to be used for heat supply, and their associated environmental effects are quite different. The logical relationship between different fuel alternatives can be found in Eq. (24) and Eq. (25).

$$Ut_{fuel} = \sum_{f=1}^F Ut_{fuel,f} \times Itcon_f \quad (24)$$

$$\sum_{f=1}^F Itcon_f = 1, 0 \leq Itcon_f \leq 1 \quad (25)$$

where $Ut_{fuel,f}$ is the amount of heat supplied by fuel f , and $Itcon_f$ is the mass fraction of fuel f ($f = \{ng, wd, oil\} \in F$).

Steam consumption comes from two parts, which are steam used in the carbon capture unit and methanol purification process, as shown in Eq. (26).

$$Ut_{stm} = \sum_{i=1}^C Ut_{stm,i} \times Itcon_i + Ut_{stm,me}, i = \{cap1, cap2, cap3, cap4\} \in C \subseteq D \quad (26)$$

where $Ut_{stm,i}$ is the amount of steam consumption for carbon capture unit i and $Ut_{stm,me}$ is the corresponding value of steam demands for unit me .

Total amount of electricity consumption Ut_{elec} is calculated in Eq. (27).

$$Ut_{elec} = Ut_{elec,me} + Ut_{elec,gf} + \sum_{i=1}^C Ut_{elec,i} \times Itcon_i, i = \{cap1, cap2, cap3, cap4\} \in C \subseteq D \quad (27)$$

where $Ut_{elec,i}$ is the amount of electricity consumption for carbon capture unit i , $Ut_{elec,me}$ is the corresponding value of power demands for unit me and $Ut_{elec,gf}$ is that for the gasification core process.

The amount of renewable electricity consumed Ut_{nelc} is supposed to be used for water electrolysis, which is calculated in Eq. (28) and Eq. (29).

$$Ut_{nelc} = \sum_{w=1}^W Ut_{nelc,w} \times Itcon_w, w = \{ew1, ew2, ew3, ew4\} \in W \subseteq D \quad (28)$$

$$\sum_{n=1}^E Itcon_n = 1, 0 \leq Itcon_n \leq 1 \quad (29)$$

where $Ut_{nelc,w}$ is the amount of renewable electricity consumption for water electrolysis unit w . $Itcon_n$ is the ratio of renewable electricity generated by source n ($n = \{soalr_{pv}, wind, solar_{tvr}, nuclear\} \in E$).

Supposing that the waste ash residues of plastic waste will be treated by landfilling. Environmental impacts associated with the transportation of plastic waste and waste ash are involved in the system boundaries. The distance of these two materials from supplier to destination is supposed to be 50 km. Freight with lorry is chosen as the transportation pathway. The number of ash residues is denoted by $Emts_{ash}$, which only originated from the gasifier, as illustrated in Eq. (30) and Eq. (31).

$$Emts_{ash} = Emts_{ash, gf} \quad (30)$$

$$trans = Mrt_{pls} \times dp + Emts_{ash} \times da \quad (31)$$

where dp is the distance of plastic waste from collection center to the treatment plant, and da is the distance of ash residue from treatment plant to the landfill. Mrt_{pls} is the mass flowrate of mixed plastic waste treated in this plant.

2.2.3. Characterization of life environmental impacts

Characterization of the direct emissions from the processes is calculated according to the ReCiPe midpoint (H) method [35], which has 18 midpoint categories. For each midpoint category, the characterization process is implemented using Eq. (32).

$$Direct_{mid} = ft_{CO2,mid}Emtg_{CO2} + ft_{NO2,mid}Emtg_{NO2} + ft_{SO2,mid}Emtg_{SO2} + ft_{twt,mid}Mtr_{twt} + ft_{wtr,mid}Mtr_{wtr} + ft_{clw,mid}Utr_{clw} + ft_{meoh,mid}Emtl_{meoh} \quad (32)$$

where $Direct_{mid}$ is the characterized value of the environmental impact mid for the direct emissions. $ft_{d,mid}$, $d = \{CO2, NO2, SO2, twt, wtr, clw, meoh\}$ is the factor of the d substance for the mid category.

For background inventory, the environmental impact per functional unit of the corresponding utilities, materials or products will be adopted directly to characterize the environmental influence. The generalized characterization function for all the background inventory is shown in Eq. (33).

$$SF_{mid,sc} = SF_{sc} \times BG_{mid,sc} \quad (33)$$

where SF_{sc} is the amount of consumption or production of substance sc , $BG_{mid,sc}$ is the value of environmental impact mid for generating per functional unit of substance sc , and $SF_{mid,sc}$ is the accumulated score. $BG_{mid,sc}$ is selected from the commercial database Ecoinvent® [36].

Noted to mention that the electricity will go through at least three-stage transformation from the power plant to the user, as depicted in Eq. (34).

$$Ut_{mid,elc} = Ut_{elec} \times (BG_{mid,elc,hp} + BG_{mid,elc,htm} + BG_{mid,elc,mvl}) \quad (34)$$

where $Ut_{mid,elc}$ is the characterized value of the environmental impact mid for the fossil-based electricity consumption. $BG_{mid,elc,hp}$ is the value of environmental impact mid for generating per functional unit of high voltage electricity, $BG_{mid,elc,htm}$ is the value of electricity voltage transformation from high voltage to medium voltage, and $BG_{mid,elc,mvl}$ is the additional burdens for transforming per functional unit of medium voltage to low voltage. Similarly, high voltage renewable electricity also goes through these transformation procedures, except for the low voltage renewable electricity produced by the solar photovoltaic technique.

The finalized characterized midpoint impact $Total_{mid}$ for the whole system is expressed in Eq. (35).

$$Total_{mid} = Direct_{mid} + Ut_{mid,elc} + Ut_{mid,nelc} + trans_{mid} + Emts_{mid,ash} + Ut_{mid,fuel} + Ut_{mid,stm} + Ut_{mid,fuel} - Prd_{mid,stm} - Prd_{mid,h2} - Prd_{mid,meoh} - Prd_{mid,elc} \quad (35)$$

2.2.4. Normalization and weighted sum

The normalized and final score for the network process is calculated in Eq. (36):

$$LCA = \sum_{mid=1}^M \frac{Total_{mid} \times norm_{mid}}{Mrt_{pls}} \quad (36)$$

where $M(mid \in M)$ is the set of all midpoint indicators, $norm_{mid}$ is the normalized factor for indicator mid , and LCA is the life cycle assessment score for the system in per kg of mixed plastic waste.

2.2.5. Uncertainty analysis

Life cycle inventory data for the energy supply superstructure (Fig. 1) are compiled from a combination of process simulations and published literature. Specifically, detailed simulation results are used for the gasification plant, while LCI data for other subsystems including carbon dioxide capture, hydrogen-to-power conversion via gas turbines, carbon dioxide utilization in methanol synthesis, and hydrogen production through various water electrolysis technologies are sourced from peer-reviewed studies and technical reports. To address the inherent uncertainties in these data and cover a wide range of industrial reality, key parameters are identified for each subsystem. These include CO_2 removal efficiencies, gas turbine energy conversion efficiencies, the H_2/CO_2 mass ratio in methanol synthesis, and the power-to-hydrogen conversion ratio for electrolysis processes. Literature values serve as best estimates, and parameter uncertainties are characterized by lognormal distributions. The pedigree matrix approach is applied to evaluate data quality and to estimate the variance of each parameter [39]. Monte Carlo simulation is implemented to propagate parameter uncertainties through the LCA model. For each simulation run, parameter values are randomly sampled from their respective distributions, and the resulting LCA outcomes are recorded. The simulation is iterated until the standard error of the mean for the primary LCA results falls below 0.003.

2.3. Surrogate model-based optimization

2.3.1. Design of experiments

The decision variables pertinent to the network model are comprehensively enumerated in Table 1. The initial quartet of these variables constitutes the fundamental operational parameters integral to the core gasification process. In contrast, the remaining variables play a pivotal

Table 1

Decision variables and their upper and lower bounds for the network model.

X	Decision variables (X)	Lower bounds (LB)	Upper bounds (UB)
x_1	steam to feed mass ratio in gasifier ($S_{gf}/Feed$)	0.5	1
x_2	steam to feed mass ratio in R-WGS ($S_{wg}/Feed$)	0.5	1
x_3	air-fuel equivalence ratio (λ)	0.1	0.5
x_4	gasifying temperature ($T_{gf}, ^\circ C$)	600	900
x_5-x_7	$Itcon_i, i = \{cap1, cap2, cap3\} \in C$	0	1
x_8-x_9	$Itcon_w, w = \{ew1, ew2\} \in W$	0	1
x_{10}^*	$fl_h, h = \{me, gt\} \in H$	0	1
x_{11}			
x_{12}^*	$Itconf, f = \{ng, wd\} \in F$	0	1
x_{13}			
x_{14}^*	$Itcon_n, n = \{soalr_{pv}, wind, solar_{tvr}\} \in E$	0	1
x_{15}			
x_{16}			

role in determining the ultimate configuration of the network. To facilitate the simulation process and derive the life cycle impact score of the network, an on-shot design of experiments methodology [40] is employed to generate a series of samples. Specifically, a full factorial design encompassing five levels is applied to the first four variables, thereby producing samples through sensitivity analysis conducted in Aspen Plus. Within each decision branch of the network, if there are n choices available, corresponding $n - 1$ independent variables are present. Consequently, there are 12 additional variables that necessitate optimization to ascertain the optimal configuration of the plastic waste valorization process. For these twelve variables, two distinct experimental design strategies are implemented. In the first strategy, these variables are treated as continuous variables, and the Latin hypercube sampling technique [41] is utilized to generate samples. It is imperative to note that during the implementation of Latin hypercube sampling, the constraints delineated in Eqs. (37)–(41) must be adhered to. To ensure comprehensive coverage of the lower and upper bounds of these decision variables, values at these bounds are incorporated into the samples, thereby forming a dataset comprising m_2 samples. In the second strategy, the twelve variables are considered as integer variables, restricted to binary values of 0 or 1. A two-level fractional factorial design [42], subject to constraints, is employed to generate m_3 samples. Consequently, the final sample size for the experimental design is determined to be $m_1 \times m_2$ and $m_1 \times m_3$. This methodological approach not only ensures a robust exploration of the decision space but also facilitates the identification of an optimal network configuration that maximizes the efficiency and sustainability of the plastic waste valorization process. The strategic application of both continuous and discrete sampling techniques underscores the comprehensive nature of the experimental design, thereby enhancing the reliability and validity of the simulation outcomes.

$$\sum_{i=1}^C Itcon_i \leq 1, i = \{cap1, cap2, cap3\} \quad (37)$$

$$\sum_{h=1}^H fh_h \leq 1, h = \{me, gt\} \quad (38)$$

$$\sum_{w=1}^W Itcon_w \leq 1, w = \{ew1, ew2\} \quad (39)$$

$$\sum_{n=1}^E Itcon_n \leq 1, n = \{soalr_{pv}, wind, solar_{lwr}\} \quad (40)$$

$$\sum_{f=1}^F Itcon_f \leq 1, f = \{ng, wd\} \quad (41)$$

3. Surrogate model training

Surrogate modeling involves a sophisticated regression process wherein the input data undergoes a non-linear transformation to yield the output. This process entails formulating an estimation of the relationship based on the observed associations between input and output data, which are derived from the experimental design [43]. Initially, the dataset was meticulously examined for duplicate values, and any redundant data entries were subsequently eliminated to ensure data integrity. Various strategies for standardizing and scaling both the predictor and response variables were optimized to enhance model performance. The original dataset was strategically divided into two subsets, allocating 90 % for training purposes and the remaining 10 % for testing. To mitigate the risk of overfitting, the k -fold cross-validation method was employed to rigorously assess the predictive accuracy of the regression model [44]. Specifically, a five-fold cross-validation approach was utilized in this study. The training data was systematically

partitioned into five distinct subsets. Within this framework, the in-fold data was reserved for model assessment, while the out-of-fold data was utilized for training purposes. root mean square error (RMSE), coefficient of determination R-squared (R^2), mean square error (MSE), and mean absolute error (MAE) were calculated for assessment of model performance [45]. Smaller values of the RMSE, MSE, and MAE are preferable, while R^2 close to 1 indicates better prediction sufficiency.

The general function of the surrogate model is formulated in Eq. (42).

$$LCA = predict(X) \quad (42)$$

where $predict(X)$ is the surrogate model used to predict the life cycle impact LCA of the network model under prediction variables matrix X, which is explained in Table 1.

Decision trees emerged as a suitable modeling technique, offering a commendable balance between accuracy and computational efficiency [46,47]. A critical hyperparameter in regression trees is the minimum leaf size, which significantly influences model performance. Additionally, the selection of sampling strategies, sample size, and scaling strategies were considered as hyperparameters within the modeling process. To optimize these hyperparameters, Bayesian optimization was employed [48,49]. The primary objective of Bayesian optimization is to identify the optimal hyperparameter values that minimize the prediction error of the surrogate model, as well as the RMSE of the test dataset. By leveraging advanced techniques such as Bayesian optimization, the study aims to enhance the predictive accuracy and robustness of the surrogate model, thereby facilitating more reliable and insightful analyses.

The objective function of hyperparameter optimization is formulated in Eq. (43).

$$obj = \alpha \times predict(X) + \theta \times RMSE(test) \quad (43)$$

where α and θ are parameters used to scale the two functions into similar magnitude. $RMSE(test)$ is the root mean square error of the testing set. Bayesian optimization is used to minimizing the obj to obtain the optimal hyperparameters.

4. Optimization based on surrogate model

The optimization strategy is illustrated in Fig. 3. This study aims to minimize the LCA value of the mixed plastic waste valorization process while simultaneously optimizing the operating conditions of the core gasification process—such as temperature, steam-to-feed ratio, equivalent ratio, and water-gas shift reaction—and the downstream supply chain structure, including decisions on unit installation. By considering the downstream supply chain structure concurrently, the decision-making process becomes more forward-looking and robust. This presents a complex mixed-integer nonlinear programming problem that requires solving intricate chemical process operations and path planning challenges. Instead of employing traditional mathematical programming methods, this research utilizes advanced machine learning techniques to develop a surrogate model for the entire network. Consequently, the optimization problem is transformed into minimizing the predictor of the surrogate model. Due to the absence of derivative information in the surrogate model, derivative-free algorithms are employed to find the minimum predictor, which serves as an approximate value of the life cycle environmental impact of the network.

The optimization problem for the green process synthesis of the plastic waste treatment process can be structured as follows:

Given:

- A set of downstream plastic waste gasification units, along with their associated utilities, material consumptions, and production outputs per functional unit.

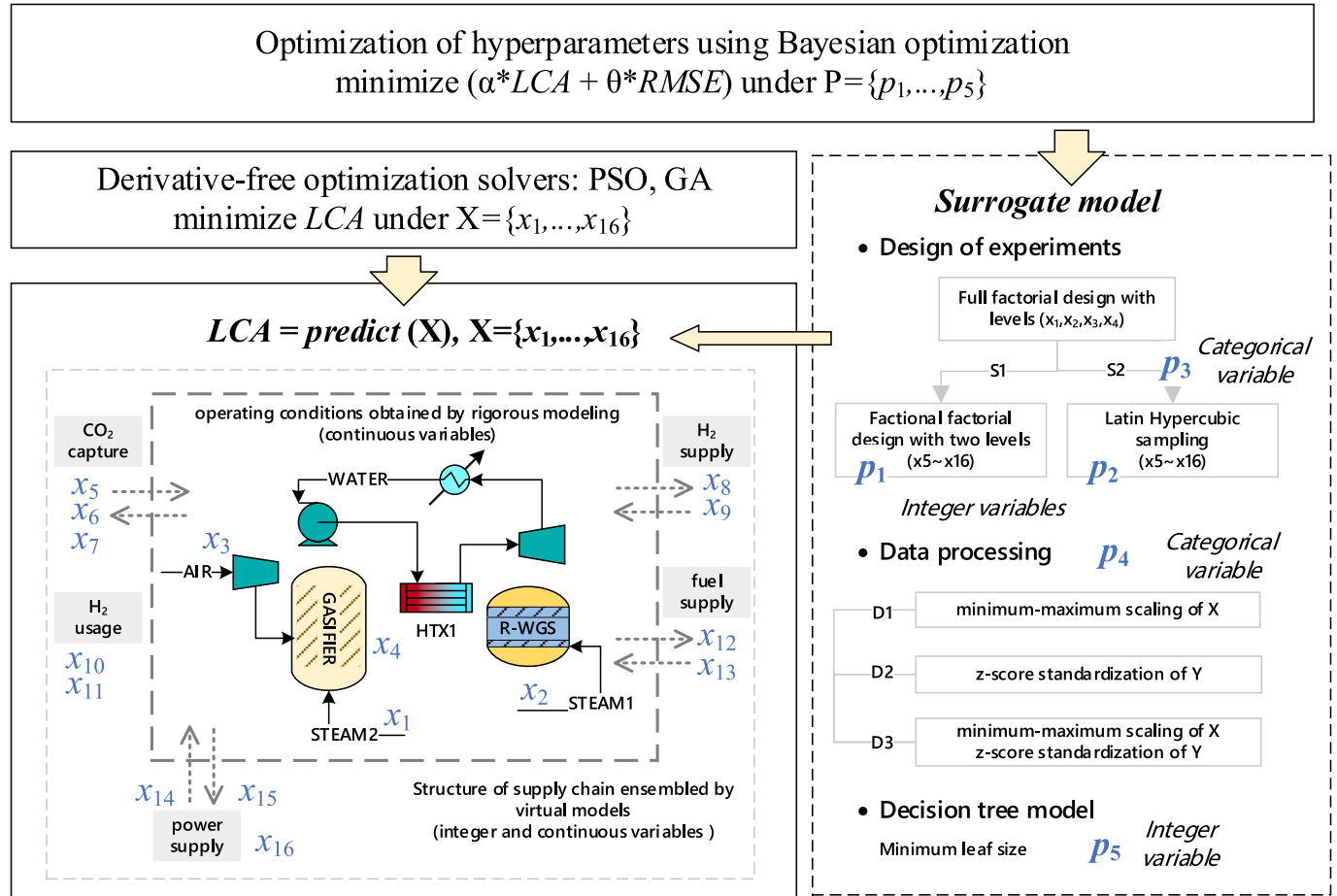


Fig. 3. Optimization strategy illustration.

- A set of available utilities and material supplies, each with their associated life cycle environmental impacts per functional unit.
- A list of operational variables for the upstream gasification process, accompanied by corresponding observations to describe the behavior of the rigorous simulation model.

Obtain:

- The optimal operational conditions for the upstream gasification process.
- The optimal configuration of the downstream energy supply chain.
- The minimum life cycle impact under the optimal operational conditions and energy supply chain configuration.

The optimization problem is formulated in (P1):

$$\begin{aligned} \min & \quad predict(X) \\ \text{s.t.} & \quad LB \leq X \leq UB \\ & \quad \text{Eqs.(37 - 41)} \\ & \quad \{x_5, x_6, x_7, x_8, x_9\} = 0 \text{ or } 1 \\ & \quad \{x_{12}, x_{13}, x_{14}, x_{15}, x_{16}\} = 0 \text{ or } 1 \end{aligned} \quad (P1)$$

Where LB and UB are the lower and upper bounds for decision variables matrix X.

Several derivative-free optimization solvers were tested in this study. For solvers which can tackle bound-constrained problems with continuous input variables, the integer constraints were transformed into continuous, as illustrated in P2.

$$\begin{aligned} \min & \quad predict(X) + penalty(X) \\ \text{s.t.} & \quad LB \leq X \leq UB \end{aligned} \quad (P2)$$

where variable matrix X needs to converge up or down to integer variables through assigning the maximum value to 1 and the rest to 0. $penalty(X)$ is the penalty function substituted for the inequality constraints, as illustrated in Eq. (44).

$$\begin{aligned} penalty = BM \times & \left(\max \left(0, \sum_{i=1}^C Itcon_i - 1 \right) + \max \left(0, \sum_{h=1}^H fh_h \right. \right. \\ & \left. \left. - 1 \right) + \max \left(0, \sum_{w=1}^W Itcon_w - 1 \right) + \max \left(0, \sum_{n=1}^E Itcon_n \right. \right. \\ & \left. \left. - 1 \right) + \max \left(0, \sum_{f=1}^F Itcon_f - 1 \right) \right) \end{aligned} \quad (44)$$

where BM is a large number.

Global optimization toolbox in MATLAB R2024b was employed for solving the optimization problem, while particle swarm optimization (PSO) was applied to problem (P2) and Genetic algorithm (GA) was used to solve problem (P1).

4.1. Case studies

To evaluate the efficiency of the proposed methodology, three case studies are designed for further comparison, as shown in Fig. 4.

Base Case: The network in the Base Case incorporates the units highlighted in Fig. 1. Five optimization scenarios of minimizing LCA, human carcinogenic toxicity (HCT, kg 1,4-DCB), global warming (GWP,

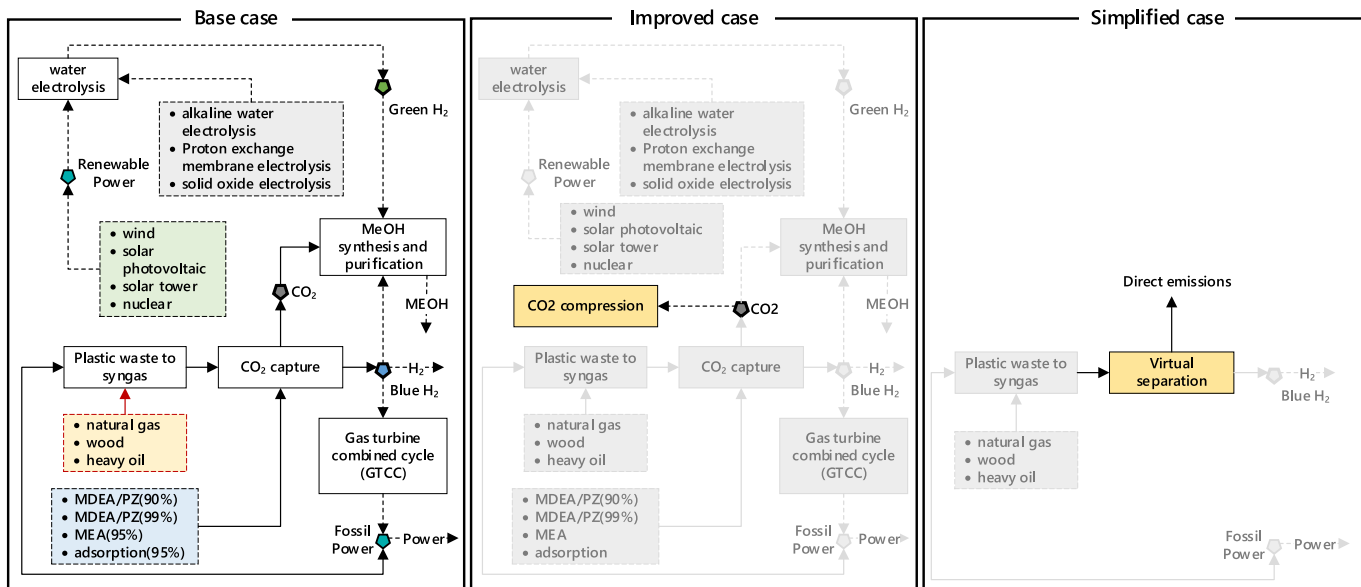


Fig. 4. Design of three case studies.

kg CO₂ eq), ozone formation affecting human health (OFH, kg NO_x eq), and terrestrial acidification (TAD, kg SO₂ eq) are performed to investigate the change of optimization results under different environmental concerns.

Improved Case: Building on the Base Case, the Improved Case

introduces an additional option for CO₂ utilization (x_{17}), which means that the captured CO₂ can be both utilized for methanol production and compression for storage. It covers two popular CO₂ utilization pathways.

Simplified Case: In the Simplified Case, carbon capture unit is not involved in the system. The product syngas from the gasification of

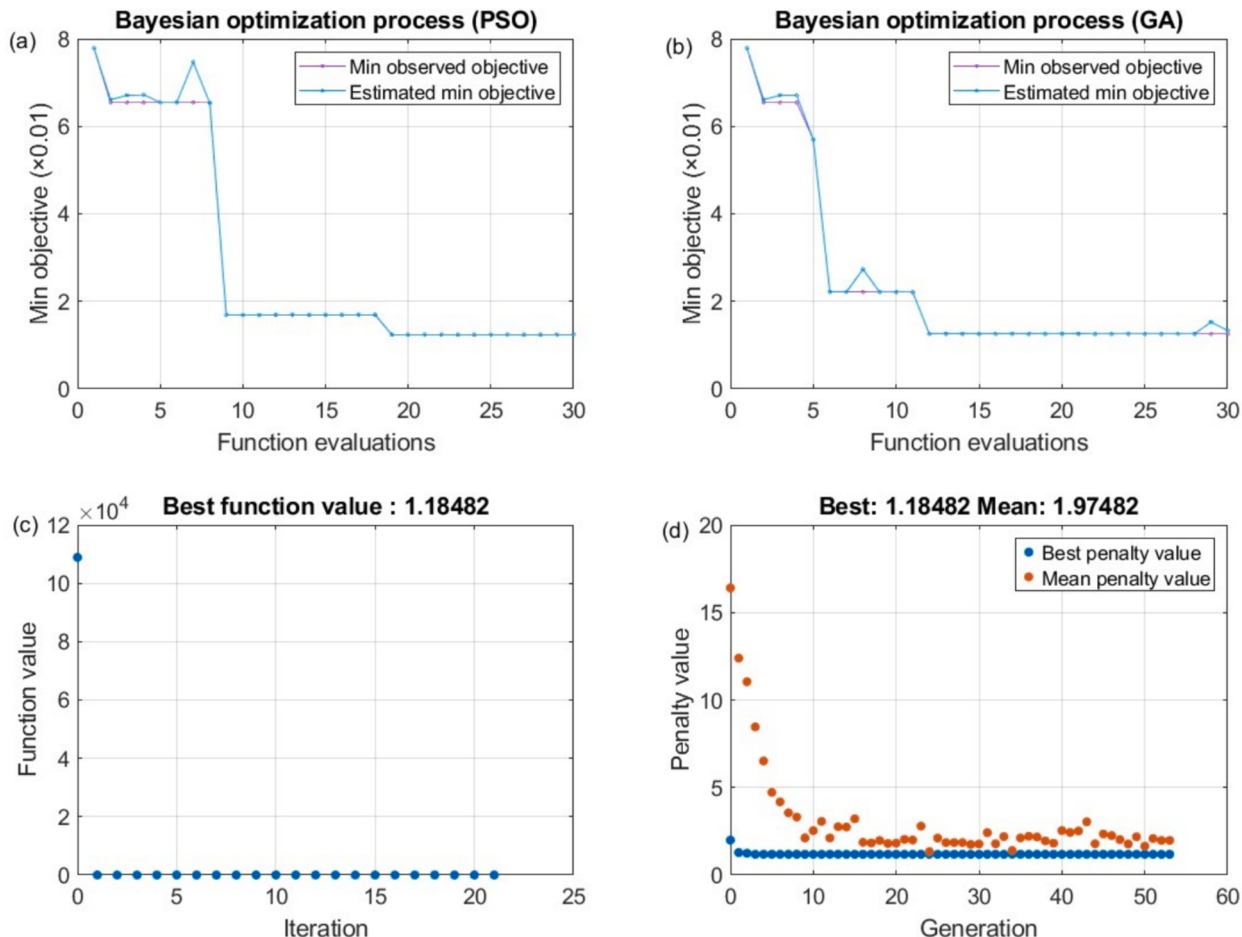


Fig. 5. Optimization process for the hyperparameters and objective LCA.

plastic waste is directly purified for hydrogen products, and the CO₂ component is emitted to the atmosphere. This case is designed to investigate the optimization performance for the operating conditions of the plastic waste to syngas process.

5. Results and discussion

5.1. Base Case

The optimization process for hyperparameter tuning is depicted in Fig. 5(a) and (b). The Bayesian optimization algorithm was employed to minimize both the LCA and the RMSE of the surrogate model. These two objectives were scaled to similar orders of magnitude. As the algorithm evaluates different sets of hyperparameters, it records the lowest objective value found so far, indicated by the line labeled "Min Observed Objectives." The line labeled "Estimated Min Objective" represents the algorithm's prediction of the minimum objective value based on a probabilistic model across the hyperparameter space, including regions that have not been explicitly evaluated. For both optimization models, the convergence of these two lines at the final evaluation suggests that the algorithm is approaching the true minimum of the objective function. The optimized hyperparameters are listed in Table 2. The minimum leaf size found for the regression tree model is 10 for the PSO-based model and 21 for the GA-based model, respectively. For the scaling and standardization of features, four strategies were designed: "y-scale" and "xy-scale" involve standardizing the output observations using the z-score function, while "x-scale" and "xy-scale" employ the minimum–maximum method for scaling the input descriptors. "none" indicates that no scaling strategies are employed, and the original data will be used directly for regression. The regression tree model can handle the original data directly. Two sampling techniques were applied: "ff" stands for the two-level fractional factorial design, and "lt" represents the Latin hypercube sampling method. "ff" was selected as the optimal sampling technique with a parameter q equal to 10 to determine the number of runs. The optimization process of the final evaluation for searching for the minimum LCA value is shown in Fig. 5(c) and (d). One hundred swarm particles and one hundred populations were used in the Particle Swarm Optimization algorithm and the Genetic algorithm, respectively. Both methods rapidly obtained the minimum LCA value, with PSO converging faster than GA within five iterations. Moreover, when validating the results in the Aspen Plus simulator, the objective obtained by PSO was slightly lower than that of GA. Therefore, PSO will be used for the subsequent analysis.

The performance of the surrogate model utilizing the optimized hyperparameters was comprehensively detailed in Fig. 6. 10 % of the dataset was reserved for testing purposes, while the remaining data underwent training and fine-fold cross-validation. The validation results for each fold for the three cases are listed in the Supplementary material (see Table S4-1 in SI). The predicted responses were plotted against the true responses for the validation dataset (Fig. 4a) and test dataset (Fig. 4c). The data points closely align with the line of perfect prediction, indicating a high level of accuracy in the model's predictions. Statistical metrics further support this observation, with a RMSE of 0.0419 and R-

squared of 0.9982, suggesting that the model explains all the variability in the response data, indicating an excellent fit. The alignment of the data points with the perfect prediction for test dataset (Fig. 4c) is consistent with the validation results (Fig. 4a), demonstrating the model's robustness and generalizability to new data. The RMSE of 0.0373 and R-squared of 0.9986 are slightly lower than those of the validation dataset, indicating even better performance on the test data. Fig. 4(b) displays the residuals between the observed and predicted values. The residuals appear randomly scattered around zero, with no discernible pattern, which is indicative of a well-fit model. The absence of systematic patterns in the residuals suggests that the model's assumptions are valid and that it does not suffer from issues such as heteroscedasticity or autocorrelation. Like the validation residuals, the test residuals (Fig. 4d) are randomly distributed around zero, further confirming the model's reliability and the absence of bias in its predictions. The consistency between the validation and test residuals plots suggests that the model maintains its performance across different datasets.

The optimized structure and critical operating parameters of the Base Case utilizing PSO algorithm are depicted in Fig. 7. Validation procedures entailed feeding the optimized operational variables into the Aspen Plus® simulator to execute the core gasification process. Subsequently, the objective function was computed. Alongside the composite environmental metrics LCA, namely HCT, GWP, OFH, and TAD, were identified as targets for minimization. Diverse optimal process configurations were thereby ascertained. In the context of evaluating the holistic environmental impact of the plastic waste treatment procedure, priority was given to the incorporation of hydrogen produced by the gasification unit in the methanol synthesis procedure, representing 51.30 % of the overall output. 37.61 % of the hydrogen output was allocated as the final product, with GTCC accounting for a mere 11.09 % of the total hydrogen yield. The surplus hydrogen product was channeled directly into the market for commercial purposes, thus engendering favorable environmental outcomes by alleviating associated burdens. An additional portion of green hydrogen, derived from proton exchange membrane electrolysis, was introduced as a reactant to methanol synthesis, constituting 65.87 % of the total hydrogen input. The integration of this green hydrogen serves to augment the sustainability profile of the overall process. In parallel, solar photovoltaic technology was chosen as the primary renewable electricity source, generating a capacity of 5144 kW. Notably, in contrast to alternative renewable electricity generation methods, electricity produced through solar photovoltaic systems operates at a lower voltage, facilitating direct consumer utilization. Conversely, other renewable energy technologies necessitate voltage transformation processes before electricity can be effectively utilized. It is worth emphasizing that factors such as production capacity limitations and natural conditions, including solar irradiation and wind speed, were excluded from the scope of this study. This deliberate omission underscores the inherent environmental advantages of solar photovoltaic technology, positioning it as the most environmentally sustainable option within the context of this study. Comparable scenarios were identified in the realm of fuel selection. The evaluation encompassed three distinct alternatives: natural gas, wood chips, and heavy oil, with the LCA score per kW of heat supply being most favorable for wood chips. Notwithstanding this, the regression model exhibited limitations in discerning between these options, with marginal relative deviations of 0.23 %, 0.17 %, and 0.55 % observed for each respective fuel choice concerning the overall LCA score. Similar limitation was found in selecting the optimal water electrolysis techniques, with an absolute error within 0.15 %. Such a margin of error was considered acceptable. The normalized midpoint values corresponding to the scenario with the least LCA impact are delineated in Section S4 of the Supporting Information.

Notably, among the 18 midpoint categories, HCT emerged as the primary contributor to the overall LCA value. Concurrently, GWP, OFH, and TAD were associated with the predominant emissions of CO₂, NO₂, and SO₂, respectively. Subsequent investigations were undertaken to

Table 2
Optimized hyperparameters for the surrogate model.

Hyperparameters	range	PSO	GA
minimum leaf in regression tree model	[1,2000]	10	21
scaling options of descriptors and observer	{"y-scale", "x-scale", "xy-scale", "none"}	"y-scale"	"y-scale"
sampling technique	{"ff", "lt"}	"ff"	"ff"
two-level fractional factorial design runs 2 ^q	[5,12]	10	10
number of samples of Latin Hypercube sampling	[1,500]	\	\

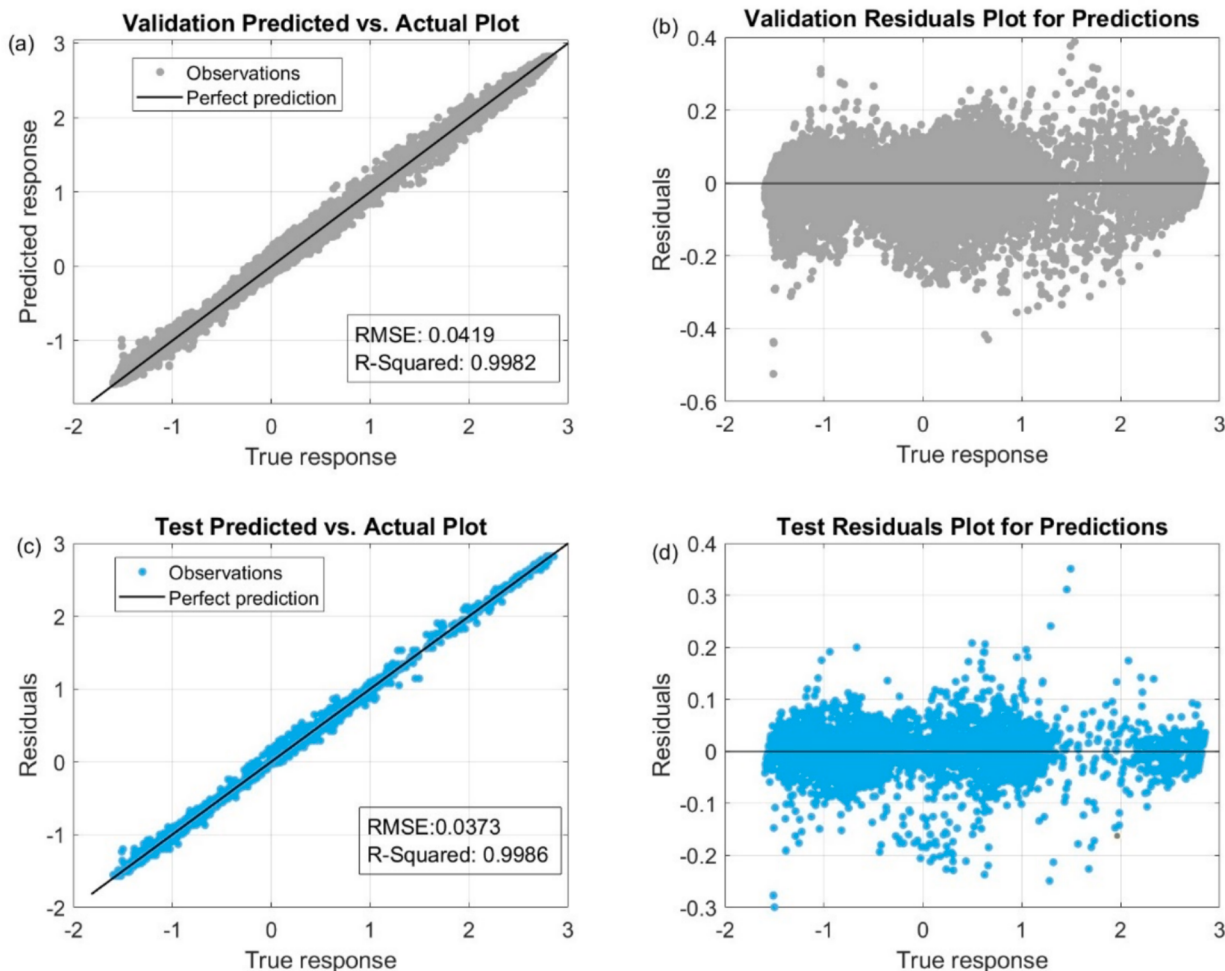


Fig. 6. Performance of the trained regression tree surrogate model.

delve into optimization strategies targeting these pivotal midpoint categories. In contrast to the foundational scenario focused on minimizing LCA, enhancements were achieved in the metrics related to HCT, GWP, OFH, and TAD by 14 %, 120 %, 26 %, and 19 %, respectively, when focusing on optimizing these individual midpoint indicators. GTCC for fossil-based electricity generation technology was deemed suboptimal for scenarios targeting the minimization of TAD. Except for this change, the optimal structure of the system was stable. The solar photovoltaic technique was identified as beneficial for all scenarios. Carbon capture technique using MDEA/PZ (90 %) was selected for minimum GWP, OFH, and TAD. When capturing 1 kg of CO₂, utilizing a mixture of MDEA/PZ under different capture rates consuming comparable amounts of electricity and cooling water utilities. However, enhancing the CO₂ capture ratio from 90 % to 99 % would directly result in a 24.21 % increase in steam consumption [31]. Adopting adsorption for CO₂ removal could significantly reduce steam consumption by 98.34 %, 93.27 %, and 90.42 % in comparison to MEA, MDEA/PZ (99 %), and MDEA/PZ (90 %), respectively. Nevertheless, transitioning from MDEA/PZ (90 %) to adsorption, MEA, and MDEA/PZ (99 %) as carbon capture techniques would lead to respective increases in GWP of 283 %, 873 %, and 78 %. This effect primarily stems from the heightened cooling water and electricity consumption associated with adsorption and MEA technologies [30]. Through a comparative analysis of the five scenarios, it was determined that negative CO₂ emissions can be achieved by increasing the mass flow rate of steam into the gasifier. This adjustment, however, results in higher heat consumption by the gasifier and an enhanced yield of hydrogen in the syngas. The scenario that minimized GWP achieved the highest hydrogen production and heat consumption among the five

scenarios. This finding aligns with the established mechanism of plastic waste gasification, which has been corroborated in other studies [28], thereby demonstrating the algorithm's efficiency to some extent. Furthermore, in the scenario focused on minimizing GWP, an optimal 64 % of the hydrogen was utilized for power generation through the unit GTCC, which produced a significantly larger amount of fossil-based power compared to the other scenarios. If the hydrogen used in GTCC is considered the final product, the GWP value would increase six-fold.

Analyzing the detailed life cycle environmental assessment results provides deeper insights into the transformations between different scenarios. Fig. 8 presents a comparative analysis of various environmental midpoint impact categories across different optimization scenarios: minimizing LCA, GWP, OFH, TAD, and HCT. Scenario "min LCA" obtains the minimum impact on freshwater, marine ecotoxicity, terrestrial ecotoxicity, human toxicity, and mineral resource. Scenario "min OFH" minimizes the stratospheric ozone depletion, ozone formation, terrestrial acidification, marine eutrophication, and land use effects simultaneously. The minimum GWP scenario exhibits the highest reduction in global warming potential, reaching nearly 100 %, indicating significant mitigation of CO₂ equivalent emissions. Fossil resource scarcity is also significantly reduced. However, this comes at the cost of significant increases in other factors. In contrast, minimizing HCT results in sacrifices in global warming potential and fossil resource scarcity. The distribution is similar for scenarios minimizing LCA and HCT. Notably, the minimum TAD achieved in the scenario minimizing TAD is slightly higher than in the scenario minimizing OFH, with an absolute error lower than 0.03 %. Among these scenarios, minimum freshwater ecotoxicity and marine eutrophication effects are achieved in

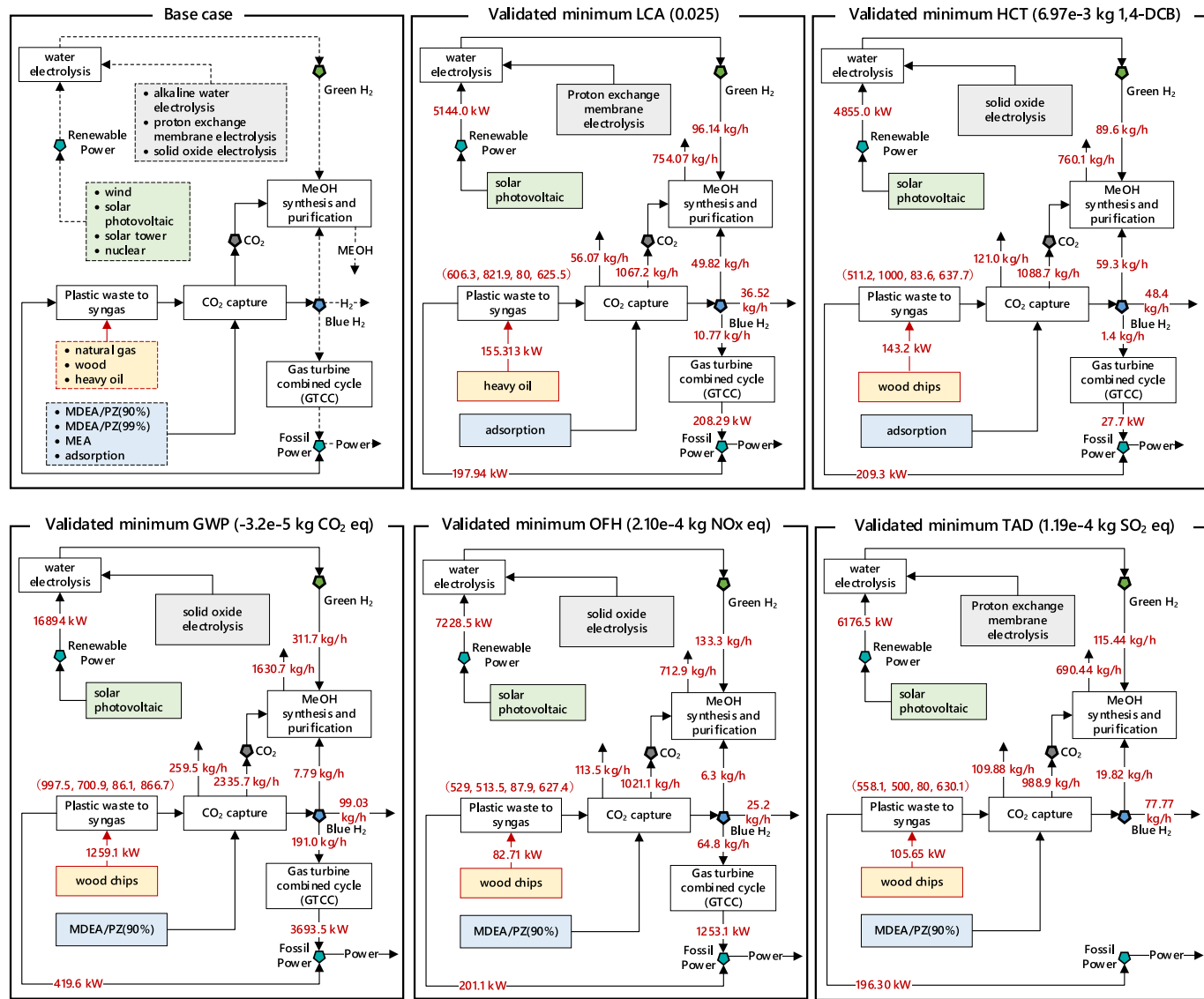


Fig. 7. Optimized operating conditions and network of Base Case.

the minimum HCT and OFH scenarios, respectively. When minimizing LCA, global warming potential and fossil resource scarcity reach their highest levels, while all other midpoint impacts peak in the min GWP scenario. Blindly pursuing minimization of GWP will sacrifice many other environmental impacts. Overall, the graph underscores the varying effectiveness of each scenario in addressing specific environmental impacts. The minimum HCT scenario is particularly effective in reducing the broadest range of impacts, including toxicity, resource scarcity, and water consumption, followed by scenario “min OFH”, which has five midpoint indicators at the lowest level. This detailed life cycle assessment provides valuable insights into the environmental trade-offs and benefits associated with each scenario, guiding strategic decision-making for sustainable development.

Shapley values, derived from cooperative game theory, are employed here to quantify the contribution of each feature to the model's predictions [50]. In regression models, predictions correspond to response values. The Shapley value of a predictor for a specific query point quantifies how much that predictor contributes to the difference between the prediction for the query point and the average prediction. The sign of the Shapley value shows whether the predictor increases or decreases the prediction, while the absolute value indicates the size of its impact. This analysis provides a comprehensive understanding of the

importance and impact of the most influential ten features on the model's output, as shown in Fig. 9. Features are ranked by their contribution, with x_{16} , x_{11} and x_3 being the most influential. Each point represents an instance in the dataset, with the color indicating the predictor value (as shown by the color scale on the right). The horizontal position of each point reflects the Shapley value, showing whether the feature contributes positively or negatively to the prediction. A positive Shapley value suggests that the feature contributes positively to the prediction, increasing the predicted value, whereas a negative Shapley value indicates a negative contribution, decreasing the predicted value. Features with a wider spread of Shapley values have a more variable impact on predictions, while those with a concentrated distribution exert a more consistent influence. For example, x_{16} and x_{11} show a wide range of Shapley values, suggesting they have a variable influence on predictions. The color gradient provides additional context, showing how different feature values affect the direction and magnitude of their contribution. Feature x_{16} represents a binary variable used to determine whether the wind power technology is installed. Variable x_{11} is a binary variable indicating the amount of hydrogen as the final product. Meanwhile, x_3 is an operating variable of the core gasification process, specifically the air molar flow rate. The length reflects the average impact of the corresponding feature on the model's predictions,

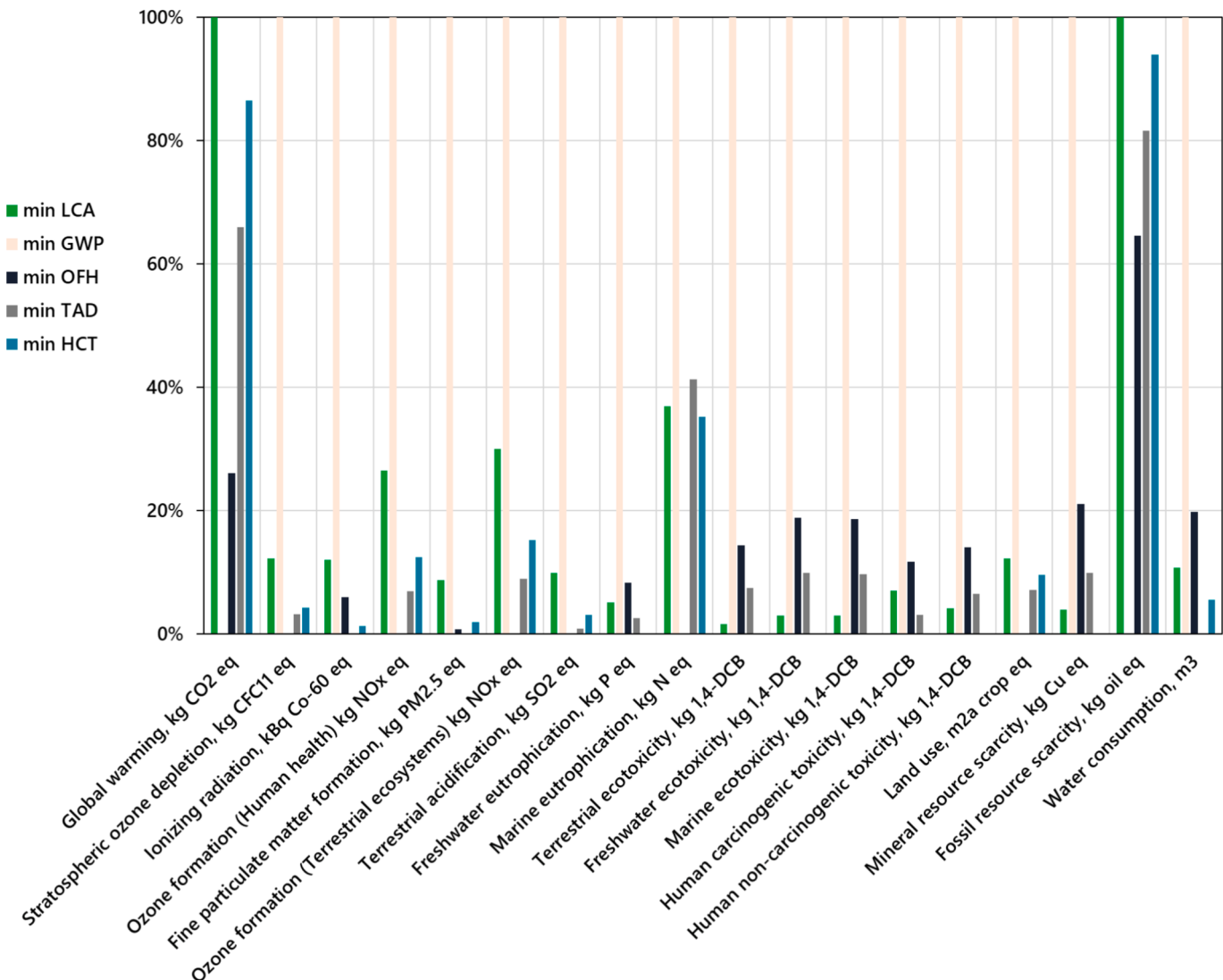


Fig. 8. Comparative analysis of the environmental assessment result under different optimization scenarios.

highlighting which features are most critical for accurate predictions. This analysis is crucial for interpreting the regression tree model, as it highlights which features are most influential in driving the model's predictions. The feature importance distribution also explains the prediction error observed. The low importance of variables x_{12} and x_{13} suggests they contribute minimally to the model, leading to reduced predictive accuracy.

5.2. Improved Case

In comparison to the Base Case, an additional option for carbon dioxide utilization has been incorporated into the network. The captured carbon dioxide can be utilized for methanol synthesis or directly processed through compression for carbon storage. In evaluating the environmental impact of the carbon dioxide compression process, only electricity consumption is considered. The optimized flowsheet structure is depicted in Fig. 10. In the scenario that minimizes the LCA, 93.39 % of the CO₂ is allocated for compression for storage, while only 6.61 % is utilized for methanol synthesis. This indicates that CO₂ compression is more advantageous than methanol synthesis. Of the hydrogen produced from the gasification process, 12.23 % is directed to the gas turbine for combustion, 58.658 % is used for methanol synthesis, and the remainder is sold as a final product. In an alternative scenario aimed at minimizing

global warming potential, renewable electricity technology is employed, resulting in a negative global warming impact. In this scenario, 81.70 % of CO₂ is compressed, and 18.30 % is used for methanol production. Compared to the Base Case, the improved scenario favors CO₂ compression, enhancing the system's environmental friendliness. The LCA and GWP values of the improved scenario are ten times lower than those of the Base Case, indicating the superiority of the additional CO₂ compression option. The decision tree model shows good accuracy for the surrogate model formulation of the Improved Case, with RMSE of the test dataset of 0.0032 and absolute residuals below 0.03, see Fig. 11. The split ratio of CO₂ (x_{17}), which determines whether the captured CO₂ is utilized for compression or for methanol synthesis, has the highest Shapley importance value. It means that the final LCA value is highly determined by the split ratio of CO₂.

5.3. Simplified Case

The Simplified Case is designed to focus only on making the main gasification process as efficient as possible, without including any of the extra equipment or steps that would normally come after it. This means it is just looking at the core part of turning plastic waste into energy and not worrying about things like capturing carbon dioxide or using the gases for other products. The optimized structure is illustrated in Fig. 12.

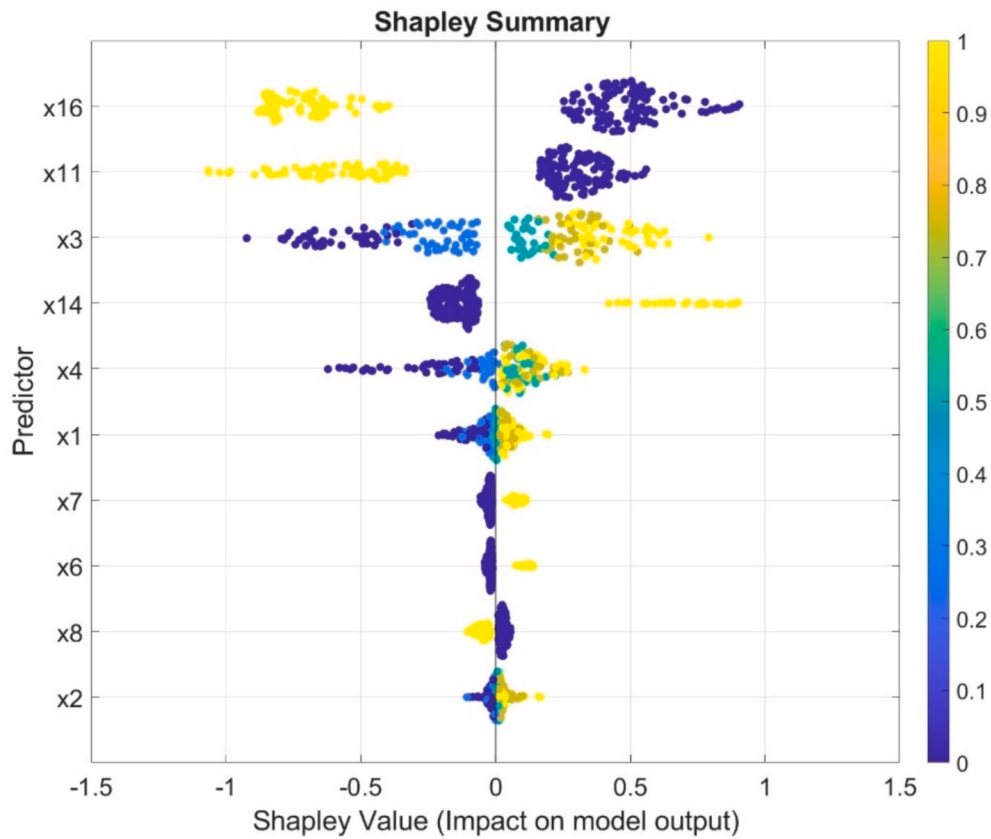


Fig. 9. Feature importance analysis of the surrogate model for LCA prediction.

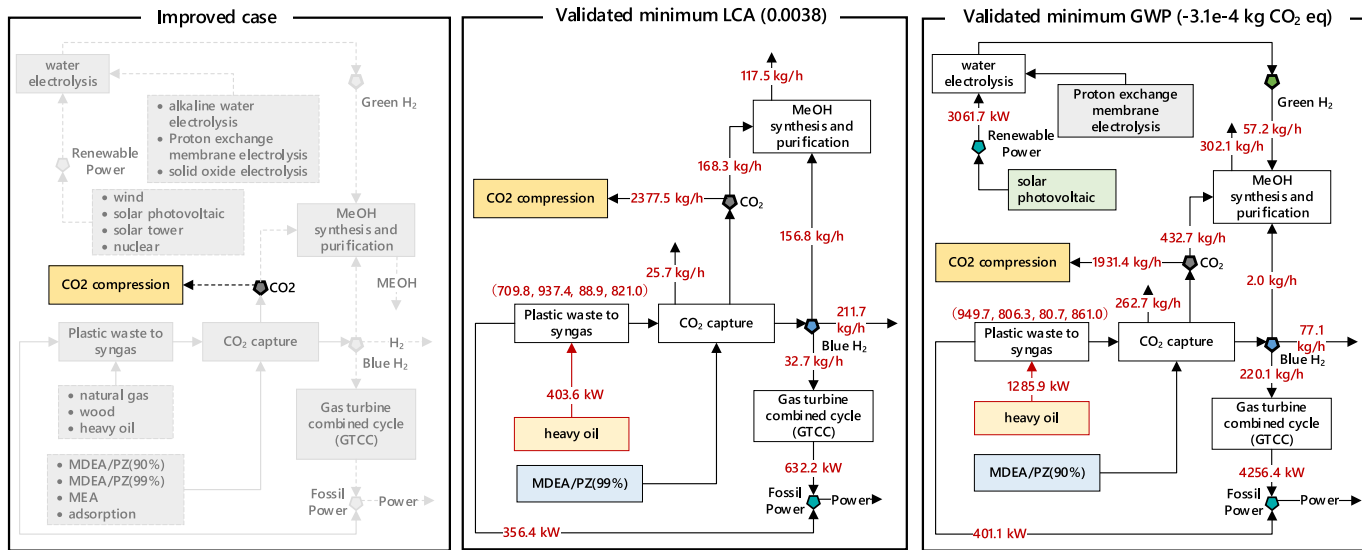


Fig. 10. Optimized operating conditions and network of Improved Case.

In addition to the gasification temperature, steam mass flow rate to the gasifier, the water-gas shift reaction, and the molar flow rate of oxygen into the gasifier, two binary variables are included to determine the optimal fuel choice. A total of six variables is optimized in this scenario. Interestingly, when looking at the normalized LCA value, the Simplified Case comes out with the lowest score compared to the other two cases. However, when looking specifically at GWP, the Simplified Case does worse than the others. This is because it doesn't include a carbon capture unit, which is very effective at reducing greenhouse gas emissions. This

result suggests something important: adding extra equipment to reduce one type of pollution (like GWP) can sometimes make other types of environmental impacts worse. For example, using more steam in the gasifier helps lower greenhouse gas emissions in the Simplified Case, but in the other cases, it has the opposite effect. The optimal steam mass flow rate for minimizing GWP is found to be 14.72 % and 13.99 % lower than that for minimizing LCA in the Base and Improved cases, respectively. However, an increase of 2.08 % is observed in the Simplified Case. Another interesting finding is that lowering the gasification temperature

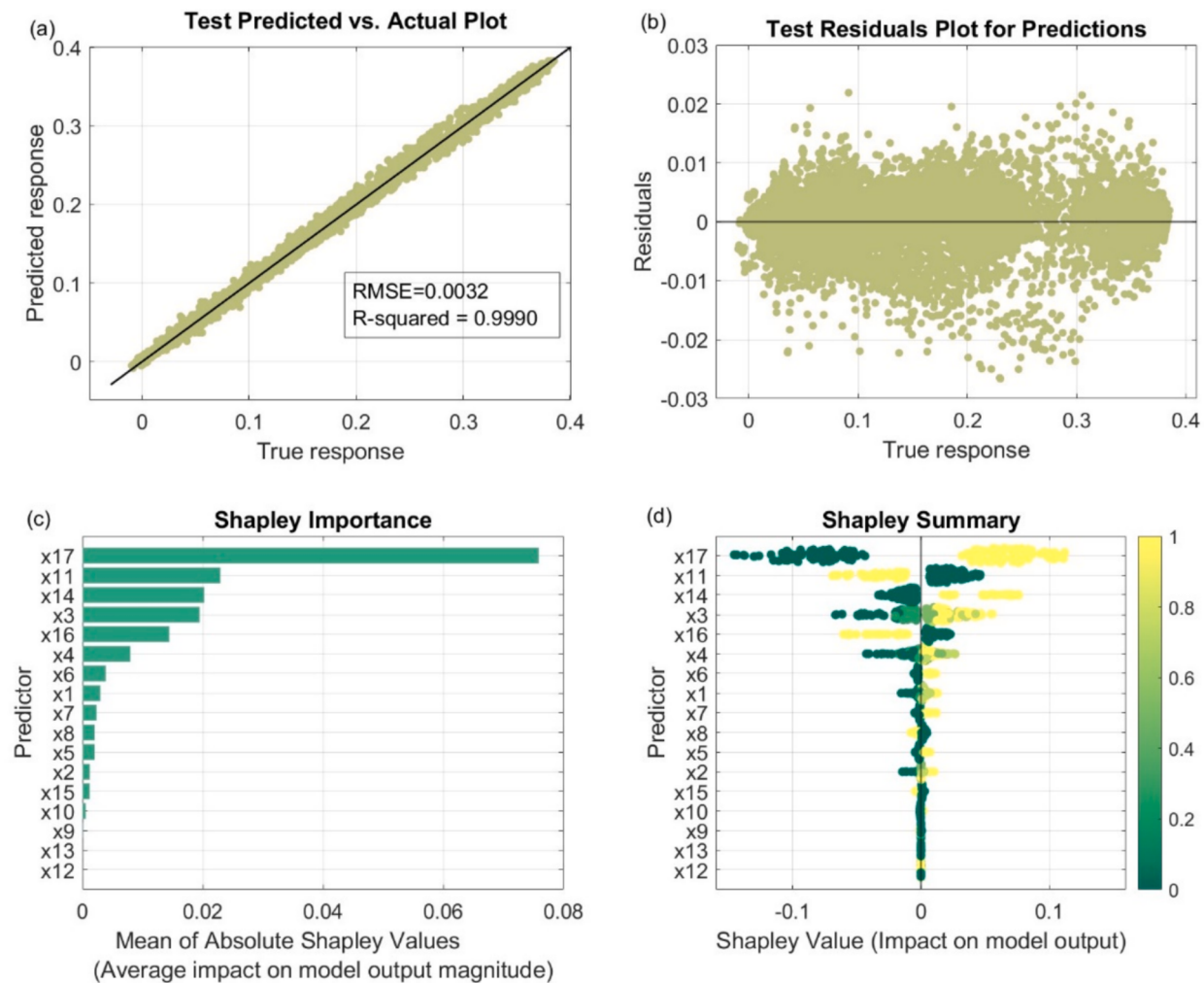


Fig. 11. Overall performance of the surrogate model for predicting LCA.

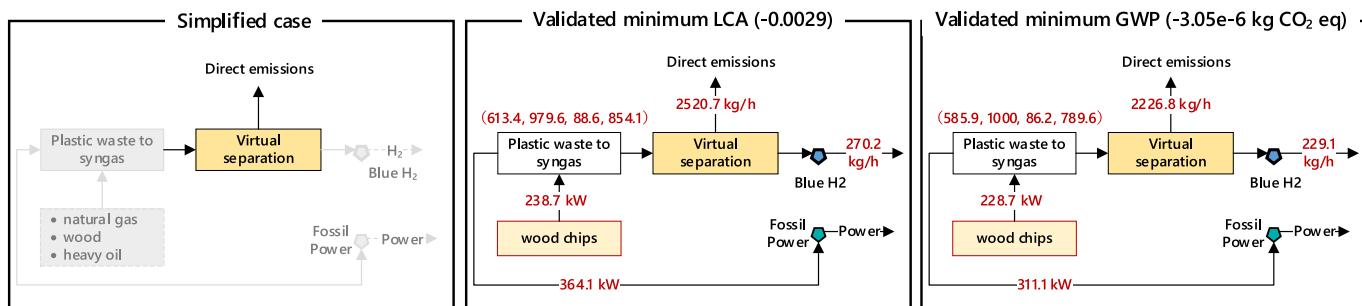


Fig. 12. Optimized operating conditions and network of Simplified Case.

helps reduce greenhouse gases in the Simplified Case, but in the other cases, you need to increase the temperature to get the same effect. This shows that the choices you make for the main process can have very different results depending on what other equipment and steps are included in the system. It is highlighted that when trying to make a process like plastic waste gasification more environmentally friendly, it's important to look at the whole system, including all the steps and equipment involved, not just the main process. Including more parts of the supply chain in the analysis gives a more complete and accurate picture of the environmental impacts and helps avoid solutions that fix one problem but make others worse.

The sample size is significantly smaller than that of the other two

cases. The RMSE of the surrogate model is approximately 0.003, and the residuals are below 0.08, indicating a strong correlation and suggesting accurate model predictions (see Fig. S4-1). An analysis of feature importance reveals that the molar flow rate of oxygen (x_3) is the determining variable for the LCA value. This variable is crucial in deciding whether the gasification reaction occurs with sufficient oxygen supply or under stoichiometric conditions, which influences whether the combustion or gasification reaction predominates. It indicates that decreasing the oxygen flowrate in plastic waste gasification plant can somehow reduce the LCA. The box plots display the range and distribution of Shapley values, with predictor x_3 showing a wide range, underscoring its substantial influence on the model's predictions.

Additionally, the choice of fuel supply (x_5 and x_6) has only a minor impact on the prediction performance (see Fig. S4-2).

5.4. Uncertainty analysis results

Uncertainty analysis was conducted for the optimal energy supply configurations of the three cases, considering a total of nine uncertain parameters. The reliability, completeness, temporal correlation, geographical correlation, and technological representativeness scores for these parameters are summarized in Table S4-4, while the calculated variances for the assumed lognormal distributions are provided in Table S4-5. As all parameters are derived from similar literature and simulation studies, their uncertainty scores are consistent across cases. For the Monte Carlo simulations, 600 samples were generated, resulting in standard errors of the mean of $2.65\text{E}-03$, $3.91\text{E}-04$, and $3.37\text{E}-19$ for the Base Case, Improved Case, and Simplified Case, respectively. The probability density functions (PDFs) and cumulative distribution functions (CDFs) obtained from these simulations are shown in Fig. S4-3. The overall results of the Monte Carlo uncertainty analysis are presented in Fig. 13, where normalized, dimensionless LCA values are displayed with error bars representing the 95 % confidence intervals. As previously discussed, the Base Case exhibits the highest normalized LCA result, with a mean value of approximately 0.025 and a relatively wide uncertainty range, indicating high sensitivity to the selected uncertain parameters. In contrast, the Improved Case shows a substantially lower mean normalized LCA result and a much narrower uncertainty range, highlighting the dominant influence of the chosen carbon dioxide utilization pathway on the LCA outcome. The Simplified Case demonstrates negligible sensitivity to the uncertain parameters, as the carbon capture, methanol synthesis, and gas turbine units are not included in the superstructure, resulting in a deterministic outcome.

6. Conclusions

In conclusion, the machine learning-based model efficiently approximates the mathematical model, predicting the environmental impact of the network with a high degree of accuracy, as evidenced by a RMSE below 0.05 and an R^2 value approaching one. Shapley importance analysis reveals that renewable power selection and hydrogen allocation influence heavily on predictions within the basic network. In the Improved Case, the selection of CO₂ usage emerges as the most significant feature, while the molar flow rate of oxygen into the gasifier becomes crucial in determining the optimal LCA value. The GWP and fossil resource scarcity impacts are optimized synergistically, though this comes at the expense of significant increases in other environmental indicators. Finally, this study highlights the potential for reducing LCA of the plastic waste valorization process by integrating various

downstream technologies. However, the optimal system structure varies significantly depending on specific environmental concerns. Minimizing one environmental indicator may lead to an increase in another. This study contributes to the advancement of environmentally responsible plastic waste valorization technologies, offering a framework for integrating machine learning and optimization techniques to address multifaceted environmental challenges. By providing a detailed analysis of the environmental implications of different optimization strategies, the research informs decision-making processes aimed at reducing the ecological footprint of plastic waste management systems. In practical scenarios, given real industrial operational data, the surrogate model developed in this study can be adapted to reflect actual plant conditions. By incorporating real LCI data, decision makers can use the proposed model to evaluate and compare different energy supply options or process configurations. This enables them to identify the optimal choices that minimize the normalized LCA value or address other specific environmental concerns relevant to their operations. Fellow researchers could employ the model and methodology to manage other emerging pollutants in environmental systems.

Although the proposed methodology demonstrates promising predictive performance and interpretability, this study has several limitations. A primary limitation is the assumption that utility consumption for each unit within the network is linearly correlated with its respective functional output. This simplification overlooks the dynamic behavior of emissions and utility consumption, which may vary under different operating conditions. Furthermore, the current model does not account for additional constraints that would enhance its practical realism, such as the variability and limitations of renewable power generation, which can be influenced by factors like solar radiation and wind speed. Future research should address these limitations by incorporating dynamic modeling of emissions and utility consumption, as well as integrating constraints related to renewable energy availability, to provide a more comprehensive and realistic assessment of network optimization.

Abbreviations

Sets

C	set of carbon capture devices
D	set of all devices
E	set of renewable power supply alternatives
F	set of fuel supply alternatives
H	set of hydrogen usage devices
W	set of water electrolysis devices

Subscript

ash	ash solid waste
cap	carbon capture unit
char	biochar
clw	water used as cooling water
elc	electricity
f	fuel choices
fuel	total fuel consumption
gf	gasification process
gh2	green hydrogen
gsf	gasifier
gt	gas turbine combined cycle
h	hydrogen utilization unit
i	carbon capture unit
me	methanol synthesis and purification unit
mid	midpoint impact categories
n	renewable power choices
nelc	renewable power consumption
pls	plastic waste
prd	final product
stm	steam
twt	water used in turbines
w	water electrolysis unit
wgs	water-gas-shift reactor
wtr	water used as feed material

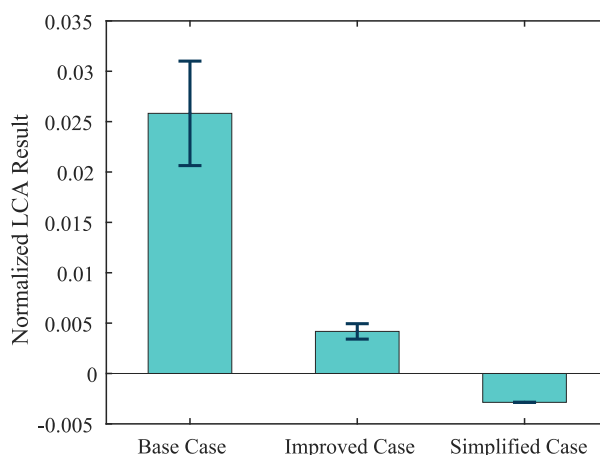


Fig. 13. Comparative uncertainty analysis results of three cases.

(continued on next page)

(continued)

Sets**Variables**

da	distance of solid waste landfilling, km
Direct	direct emissions
dp	distance of plastic waste sources, km
Emtg	direct gaseous emissions, kg
Emtl	direct liquid emissions, kg
Emts	direct solid emissions, kg
fh	mass ratio of hydrogen
ft	factor to calculate the midpoint impact
hhv	higher heating value, MJ/kg
IIcon	integer variables of equipment
LCA	average sum score
Mas	mass quantity, kg
Mtr	material consumption, kg
norm	normalization factor
Prd	product stream
Syn	syngas produced by the gasification
Total	characterized midpoint impact
trans	transportation of raw materials, kg·km
Ut	utilities consumption

CRediT authorship contribution statement

Qiming Qian: Writing – original draft, Visualization, Software, Data curation. **Yusha Hu:** Writing – original draft, Software, Conceptualization. **Jingzheng Ren:** Supervision, Investigation, Funding acquisition, Conceptualization. **Chang He:** Writing – review & editing, Software, Conceptualization.

Declaration of competing interest

The authors declare that they have no known competing financial interests or personal relationships that could have appeared to influence the work reported in this paper.

Acknowledgements

The work described in this paper was supported by a grant from the Research Committee of The Hong Kong Polytechnic University under student account code RKQ6. The authors would like to express their sincere thanks to the financial support from the Research Institute for Advanced Manufacturing (RIAM) of The Hong Kong Polytechnic University (project code: 1-CDK2, Project ID: P0050827). It is also supported by a grant from the Environment and Conservation Fund (ECF) (Project ID: P0043333, Funding Body Ref. No: ECF 51/2022, Project No. K-ZB5Z), a grant from Research Grants Council of the Hong Kong Special Administrative Region, China-General Research Fund (Project ID: P0046940, Funding Body Ref. No: 15305823, Project No. B-QC83), and a grant from the PROCORE-France/Hong Kong Joint Research Scheme sponsored by the Research Grants Council of Hong Kong and the Consulate General of France in Hong Kong (Ref. No. F-PolyU501/22 for the Hong Kong part and 49387ZA for the French part).

Appendix A. Supplementary data

Supplementary data to this article can be found online at <https://doi.org/10.1016/j.enconman.2025.120416>.

Data availability

Data will be made available on request.

References

- [1] OECD – processed by Our World in Data. Global Plastic Outlook. 2022.
- [2] Yadav G, Singh A, Dutta A, Uekert T, DesVeaux JS, Nicholson SR, et al. Techno-economic analysis and life cycle assessment for catalytic fast pyrolysis of mixed plastic waste. Energy Environ Sci 2023. <https://doi.org/10.1039/d3ee00749a>.
- [3] Falascino E, Joshi RK, Kumar S, Jawdekar T, Kudva IK, Shinde SG, et al. Enabling plastic waste gasification by autothermal chemical looping with > 90 % syngas purity for versatile feedstock handling. Appl Energy Combust Sci 2024;19:100270. <https://doi.org/10.1016/j.jaecs.2024.100270>.
- [4] Abedin A, Bai X, Muley P. Microwave-assisted catalytic gasification of mixed plastics and corn stover for low tar, hydrogen-rich syngas production. Int J Hydrogen Energy 2024;77:69–83. <https://doi.org/10.1016/j.ijhydene.2024.06.176>.
- [5] Zou J, Zhao L, Hu Q, Yao D, Yang H. Pyrolysis and catalytic reforming of disposable plastic waste for syngas production with adjustable H₂/CO ratio. Appl Energy 2024;362:122844. <https://doi.org/10.1016/j.apenergy.2024.122844>.
- [6] Parrillo F, Ardolino F, Cali G, Pettinai A, Materazzi M, Sebastiani A, et al. Plastic waste gasification using oxygen-enriched air and steam: Experimental and model results from a large pilot-scale reactor. Waste Manag 2024;183:53–62. <https://doi.org/10.1016/j.wasman.2024.04.045>.
- [7] Han SW, Lee JJ, Tokmurzin D, Lee SH, Nam JY, Park SJ, et al. Gasification characteristics of waste plastics (SRF) in a bubbling fluidized bed: Effects of temperature and equivalence ratio. Energy 2022;238:121944. <https://doi.org/10.1016/j.energy.2021.121944>.
- [8] Jeon S, Farooq A, Lee IH, Lee D, Seo MW, Jung S-C, et al. Green conversion of wood plastic composites: A study on gasification with an activated bio-char catalyst. Int J Hydrogen Energy 2024;54:96–106. <https://doi.org/10.1016/j.ijhydene.2023.05.127>.
- [9] Mishra R, Shu C-M, Gollakota ARK, Pan S-Y. Unveiling the potential of pyrolysis-gasification for hydrogen-rich syngas production from biomass and plastic waste. Energy Convers Manag 2024;321:118997. <https://doi.org/10.1016/j.enconman.2024.118997>.
- [10] Terlouw T, Bauer C, McKenna R, Mazzotti M. Large-scale hydrogen production via water electrolysis: a techno-economic and environmental assessment. Energy Environ Sci 2022;15:3583–602. <https://doi.org/10.1039/D2EE01023B>.
- [11] Wang X, Sha L, Hu S, Li Z, Guo H, Zhang J, et al. A techno-economic study of photovoltaic-solid oxide electrolysis cell coupled magnesium hydride-based hydrogen storage and transportation toward large-scale applications of green hydrogen. Energy Environ Sci 2024;17:8429–56. <https://doi.org/10.1039/D4EE04224G>.
- [12] Postweiler P, Engelpracht M, Rezo D, Gibelhaus A, von der Assen N. Environmental process optimisation of an adsorption-based direct air carbon capture and storage system. Energy Environ Sci 2024;17:3004–20. <https://doi.org/10.1039/D3EE02970K>.
- [13] Terlouw T, Bauer C, Rosa L, Mazzotti M. Life cycle assessment of carbon dioxide removal technologies: a critical review. Energy Environ Sci 2021;14:1701–21. <https://doi.org/10.1039/D0EE03757E>.
- [14] Abouemara K, Shahbaz M, Boulfrad S, McKay G, Al-Ansari T. Design of an integrated system that combines the steam gasification of plastic waste and a solid oxide fuel cell for sustainable power generation. Energy Convers Manage: X 2024; 21:100524. <https://doi.org/10.1016/j.ecmx.2024.100524>.
- [15] Prifti K, Lechtenberg F, Manenti F, Espuña A, Graells M. Comparing the climate impact of methanol production in Europe: steam methane reforming vs. Plastic waste gasification processes. Resour Conserv Recycl 2024;208:107653. <https://doi.org/10.1016/j.resconrec.2024.107653>.
- [16] Laky DJ, Cortes NP, Eslick JC, Noring AA, Susarla N, Okoli C, et al. Market optimization and technoeconomic analysis of hydrogen-electricity coproduction systems. Energy Environ Sci 2024;17:9509–25. <https://doi.org/10.1039/D4EE02394C>.
- [17] Hernández B, Vlachos DG, Ierapetritou MG. Superstructure optimization for management of low-density polyethylene plastic waste; Electronic supplementary information (ESI) available. See DOI: <https://doi.org/10.1039/d4gc00339j>. Green Chemistry 2024;26:9476–87. 10.1039/d4gc00339j.
- [18] Graham EJ, Sheha M, Mallapragada DS, Herzog HJ, Gencer E, Cross P, et al. Optimization of a combined power plant CO₂ capture and direct air capture concept for flexible power plant operation. Energy Environ Sci 2024;17:4157–74. <https://doi.org/10.1039/D4EE00309H>.
- [19] Zare AAD, Yari M. Comprehensive examination and analysis of thermodynamics in a multi-generation hydrogen, heat, and power system based on plastic waste gasification integrated biogas-fueled chemical looping combustion. Process Saf Environ Prot 2024;183:976–91. <https://doi.org/10.1016/j.psep.2024.01.060>.
- [20] Gassner M, Vogel F, Heyen G, Maréchal F. Optimal process design for the polygeneration of SNG, power and heat by hydrothermal gasification of waste biomass: process optimisation for selected substrates. Energy Environ Sci 2011;4: 1742–58. <https://doi.org/10.1039/C0EE00634C>.
- [21] Mencarelli L, Chen Q, Pagot A, Grossmann IE. A review on superstructure optimization approaches in process system engineering. Comput Chem Eng 2020; 136. <https://doi.org/10.1016/j.compchemeng.2020.106808>.
- [22] Taipabu MI, Huang C-M, Irfan HM, Viswanathan K, Adi VSK, Wu W. Superstructure optimization of hydrothermal liquefaction for microalgae biorefinery considering environmental impacts and economics. Renew Energy 2024;237:121593. <https://doi.org/10.1016/j.renene.2024.121593>.
- [23] Shirasaki S, Pishvaei MS, Sobati MA. Integrated supply chain network design and superstructure optimization problem: A case study of microalgae biofuel supply chain. Comput Chem Eng 2024;180:108468. <https://doi.org/10.1016/j.compchemeng.2023.108468>.

- [24] Huynh D, Ierapetritou M. Biorefinery superstructure optimization under carbon pricing policies using stochastic programming. *Appl Energy* 2024;376:124283. <https://doi.org/10.1016/j.apenergy.2024.124283>.
- [25] Eh CLM, Tiong ANT, Lim CH, Kansedo J, How BS, Ng WPQ. A MILP model for integrated circular hydrogen economy based in Malaysia with intermodal transportation. *Int J Hydrogen Energy* 2024;92:1320–34. <https://doi.org/10.1016/j.ijhydene.2024.10.319>.
- [26] Abu Salem K, Palaia G, Quarta AA. Review of hybrid-electric aircraft technologies and designs: critical analysis and novel solutions. *Prog Aerosp Sci* 2023;141:100924. <https://doi.org/10.1016/j.paerosci.2023.100924>.
- [27] Yan Y, Borhani TN, Subraveti SG, Pai KN, Prasad V, Rajendran A, et al. Harnessing the power of machine learning for carbon capture, utilisation, and storage (CCUS) – a state-of-the-art review. *Energy Environ Sci* 2021;14:6122–57. <https://doi.org/10.1039/D1EE02395K>.
- [28] Qian Q, Ren J, He C, Azzaro-Pantel C. Approaching circular economy through waste-to-blue hydrogen: Systems modeling and multi-objective optimization. *Chem Eng J* 2024;497:154660. <https://doi.org/10.1016/j.cej.2024.154660>.
- [29] Jang D, Kim J, Kim D, Han W-B, Kang S. Techno-economic analysis and Monte Carlo simulation of green hydrogen production technology through various water electrolysis technologies. *Energy Convers Manag* 2022;258:115499. <https://doi.org/10.1016/j.enconman.2022.115499>.
- [30] Zhou X, Liu J, Yan H, Feng X, Liu Y, Yang C, et al. Multi-dimensional assessment for the novel carbon capture process integrated the low-temperature adsorption and desorption. *Chem Eng Sci* 2023;282:119207. <https://doi.org/10.1016/j.ces.2023.119207>.
- [31] Kum J, Oh H-T, Park J, Kang J-H, Lee C-H. Techno-economic analysis and optimization of a CO₂ absorption process with a solvent looping system at the absorber using an MDEA/PZ blended solvent for steam methane reforming. *Chem Eng J* 2023;455:140685. <https://doi.org/10.1016/j.cej.2022.140685>.
- [32] Qian Q, Ren J, He C. Plastic waste upcycling for generation of power and methanol: process simulation and energy-exergy-economic (3E) analysis. *Ind Eng Chem Res* 2023;62:17857–70. <https://doi.org/10.1021/acs.iecr.3c02665>.
- [33] The International Standards Organization. Environmental management — life cycle assessment — principles and framework. ISO 14040 2006. International Organization for Standardization; 2006.
- [34] The International Standards Organization. International standard assessment — requirements and guidelines, ISO 14044. International Organization for Standardization; 2006.
- [35] Huijbregts MAJ, Steinmann ZJN, Elshout PMF, Stam G, Verones F, Vieira M, et al. ReCiPe2016: a harmonised life cycle impact assessment method at midpoint and endpoint level. *Int J Life Cycle Assess* 2017;22:138–47. <https://doi.org/10.1007/s11367-016-1246-y>.
- [36] Wernet G, Bauer C, Steubing B, Reinhard J, Moreno-Ruiz E, Weidema B. The ecoinvent database version 3 (part I): overview and methodology. *Int J Life Cycle Assess* 2016;21:1218–30.
- [37] Qian Q, Ren J. From plastic waste to potential wealth: Upcycling technologies, process synthesis, assessment and optimization. *Sci Total Environ* 2024;907:167897. <https://doi.org/10.1016/j.scitotenv.2023.167897>.
- [38] The Engineering ToolBox. Fuels - Higher and Lower Calorific Values 2003. https://www.engineeringtoolbox.com/fuels-higher-calorific-values-d_169.html (accessed October 16, 2024).
- [39] Goedkoop M, Oele M, Leiting J, Ponsioen T, Meijer E. Introduction to LCA with SimaPro. 2016.
- [40] Román-Ramírez LA, Marco J. Design of experiments applied to lithium-ion batteries: A literature review. *Appl Energy* 2022;320:119305. <https://doi.org/10.1016/j.apenergy.2022.119305>.
- [41] Song C, Kawai R. Monte Carlo and variance reduction methods for structural reliability analysis: A comprehensive review. *Probab Eng Mech* 2023;73:103479. <https://doi.org/10.1016/j.probengmech.2023.103479>.
- [42] Carlson R, Carlson JE, editors. Chapter 6 Two-level fractional factorial designs. Design and optimization in organic synthesis, vol. 24, Elsevier; 2005, p. 119–68. 10.1016/S0922-3487(05)80010-3.
- [43] Williams B, Cremaschi S. Novel Tool for Selecting Surrogate Modeling Techniques for Surface Approximation. In: Türkay M, Gani R, editors. 31st European Symposium on Computer Aided Process Engineering, vol. 50, Elsevier; 2021, p. 451–6. 10.1016/B978-0-323-88506-5.50071-1.
- [44] Malakouti SM. Improving the prediction of wind speed and power production of SCADA system with ensemble method and 10-fold cross-validation. *Case Stud Chem Environ Eng* 2023;8:100351. <https://doi.org/10.1016/j.cscee.2023.100351>.
- [45] Das PK, Sahu RL, Swain PC. Comparative analysis of machine learning models for rainfall prediction. *J Atmos Sol Terr Phys* 2024;264:106340. <https://doi.org/10.1016/j.jastp.2024.106340>.
- [46] Aittchakouchi T, Elkari B, Chaibi Y, Kousksou T. Random forest with feature selection and K-fold cross validation for predicting the electrical and thermal efficiencies of air based photovoltaic-thermal systems. *Energy Rep* 2024;12:988–99. <https://doi.org/10.1016/j.egyr.2024.07.002>.
- [47] Saad M, Zhang Y, Jia J, Tian J. Decision tree-based approach to extrapolate life cycle inventory data of manufacturing processes. *J Environ Manage* 2024;360:121152. <https://doi.org/10.1016/j.jenvman.2024.121152>.
- [48] Asante-Okyere S, Shen C, Osei H. Enhanced machine learning tree classifiers for lithology identification using Bayesian optimization. *Appl Comput Geosci* 2022;16:100100. <https://doi.org/10.1016/j.acags.2022.100100>.
- [49] Alruqi M. Optimizing the model-prediction of date palm fronds-derived producer gas and third generation biodiesel powered dual-fuel engine by employing Bayesian-optimized Boosted Regression Trees for enhanced prognostics. *Process Saf Environ Prot* 2024;187:1338–53. <https://doi.org/10.1016/j.psep.2024.05.036>.
- [50] Jiang J, Xiang X, Zhou Q, Zhou L, Bi X, Khanal SK, et al. Optimization of a novel engineered ecosystem integrating carbon, nitrogen, phosphorus, and sulfur biotransformation for saline wastewater treatment using an interpretable machine learning approach. *Environ Sci Technol* 2024;58:12989–99. <https://doi.org/10.1021/acs.est.4c03160>.